ACS OMEGA

Open Access

http://pubs.acs.org/journal/acsodf

Article

Paleoenvironmental Settings of the Soma Coal Basin (Turkey): Insights from Maceral Data, Biomarker, and Carbon Isotopic Composition

Selin Karadirek*

Cite This: *ACS Omega* 2023, 8, 47974−47990

Read Online

ACCESS | Metrics & More | Article Recommendations

ABSTRACT: Organic geochemical (TOC, pyrolysis, biomarker) and petrographic (maceral analysis) investigations together with organic carbon isotope studies were carried out to characterize in detail the depositional environment, determine the organic matter type, and assess the hydrocarbon production potential of three coal seams (KP1-upper, KM3-middle, and KM2-lower) in the Soma (Manisa, Western Anatolia) coal field in Turkey. The total organic carbon value of the upper coal seam ranged between 11.7 and 55.75%, the middle coal seam between 20.12 and 62.86%, and the lower coal seam between 50.03 and 65.71%. Coals in all three seams are characterized by low hydrogen index (HI) values (<151 mg HC/g TOC), low bitumen index (BI) (<19 g HC/g TOC), and quality index (QI) between 23 and 156 mg HC/g TOC. According to Rock-Eval pyrolysis data, the organic matter type of the coals is type III kerogen. Huminite reflectance, Tmax, and biomarker data (22S/22S+22R (C_{32}) sterane, $\beta\beta/(\alpha\alpha + \beta\beta)$ (C_{29}) sterane, and MPI-1) indicate that the organic matter is not thermally mature and that the Soma-Manisa coal has reached the sub-bituminous rank. Rock-Eval data shows that coal is gas-prone and has not reached the maturity threshold required for initial gas production. The dominant maceral group is huminite while liptinite and inertinite macerals have been found in minor amounts. Groundwater index (GWI), vegetation index (VI), tissue preservation index (TPI), and gelification index (GI) parameters indicate a transition from limnic-limno-telmatic to limno-telmatic-telmatic environment from the upper seam to the lower seam. *N*-Alkane distributions show that paleoclimatic conditions have changed from KP1 to KM2. The higher abundance of pristane compared to phytane and low $C_{35}/C_{31}-C_{35}$ homohopane index values demonstrate that the coals were deposited in a suboxic−oxic environment. The predominance of *n*-alkanes with generally high carbon number, relative variable abundances of $C_{27}-C_{28}-C_{29}$ steranes, $\delta^{13}C$ values, C/N ratios, and very low gammacerane index indicate a terrestrial ecosystem with nonmarine influence, although algae and microorganisms also contributed to the biomass.

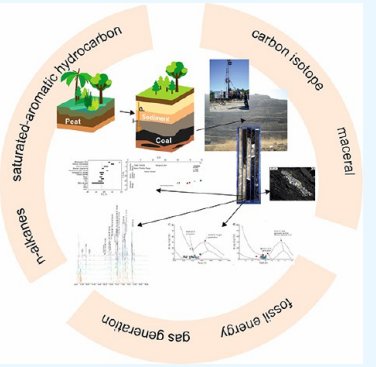

1. INTRODUCTION

Coal has the second largest share after oil in the distribution of the world's primary energy supply by sources.[1] Lignite constitutes 93% of Turkey's total coal reserves.[2] Moreover, lignite is of economic importance, as it represents the main source of electricity generation. As a result of favorable peat formation conditions, lignite basins with large coal reserves (such as Karapınar-Konya, Alpu-Eskişehir, Elbistan-Kahramanmaraş, Silivri-stanbul, Soma-Manisa, and Dinar-Afyonkarahisar) were formed during the Neogene in Turkey.

The first studies on the Soma-Manisa coal basin were conducted by Brinkmann et al.,[3] Nebert,[4] and Cetin[5] on the structural geology and lithostratigraphy of the region. After the identification of three coal seams of Neogene age in the basin, namely, upper (KP1), middle (KM3), and lower (KM2), studies were carried out to determine the composition, distribution, and depositional conditions of the coals by examining mainly the organic petrography and mineralogical and chemical compositions of the coal in different seams.[6−15] There is a limited organic geochemical evaluation in the KM2 seam by Yasar[16] and Karadirek and Ozcelik,[17] and in the KP1 and KM3 seams, mainly in the KM2 seam by Oskay et al.[18]

Nowadays, it has become important to reassess the vegetation community and paleoenvironmental−paleoclimatic conditions in peatlands through extensive research with biomarker analysis from extractable organic matter (EOM) extracted from coals.[19−25] Since the coal formation process can be influenced by many natural factors,[20] it should be supported by other data in addition to organic geochemical parameters. Reconstruction of paleoclimate based on *n*-alkane distributions has been widely applied in peat deposits.[26,27] However, these studies were

Received: September 3, 2023
Revised: November 19, 2023
Accepted: November 23, 2023
Published: December 5, 2023

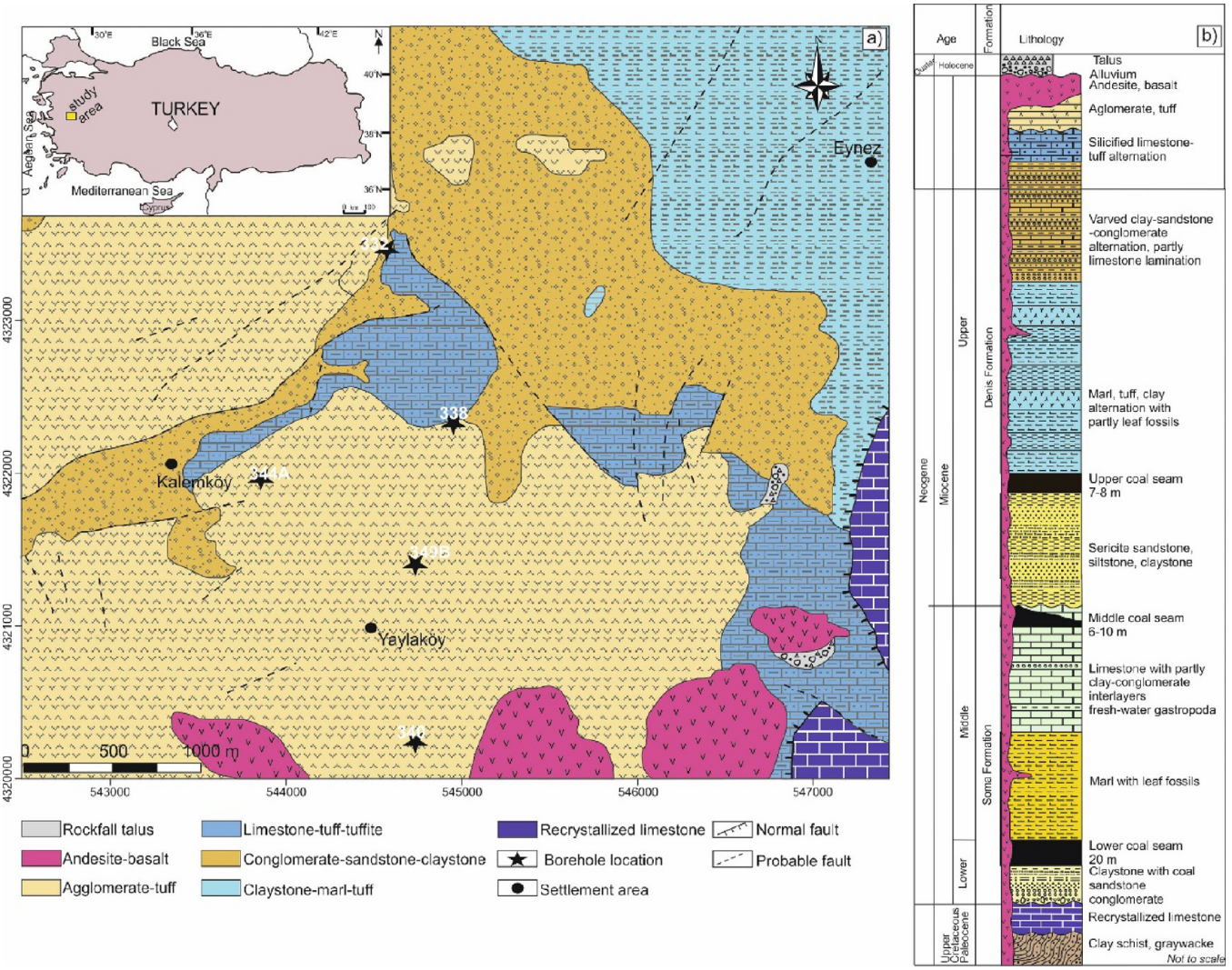

Figure 1. (a) Geological map of Soma-Manisa. (b) Stratigraphic column of Soma-Manisa. (adapted with permission from ref 17. Copyright 2019 ACS.,[13, 17])

limited to lignite deposits.[21,28] Mathews et al.[21] determined the paleoclimatic characteristics of the Early Paleogene Barsingsar lignite-bearing Sequence of Rajasthan based on stable carbon isotope data along with biomarker distributions. This study aims to evaluate and compare the organic matter sources and depositional environment characteristics of the upper, middle, and lower coal seams in the Soma-Manisa coal basin in detail and to estimate the hydrocarbon potential in these three seams. Extensive organic geochemical, stable carbon isotope, and maceral distribution analyses were performed to achieve this objective.

2. GEOLOGICAL BACKGROUND

The Soma basin is one of the basins formed in the NE−SW-trending and fault-bounded depressions in Western Anatolia following the collision of the Sakarya Zone and the Anatolian Block between the Early Miocene and the Early Pliocene. After the Pliocene, due to regional uplift, tensional stresses that led to the formation of approximately E−W-trending grabens were effective in all Western Anatolia. Basaltic volcanism, which was active in the region in the late Pliocene/early Quaternary, developed in connection with this graben formation.[3,29] The study area within the Soma coal basin is located approximately 15 km southwest of Soma-Manisa (Figure 1a). Therefore, coal formations in the Soma region developed both under the influence of the extensional tectonic regime and due to volcanic activities.[4,30] Mesozoic-aged graywacke and shale rocks and recrystallized limestones are the basement rocks of the region (Figure 1b). Miocene sediments (Soma and Deniş Formations) are discordant on these basement rocks. Lower-Middle Miocene and Upper Miocene sediments indicate two separate sedimentary depositional phases that are erosionally separated from each other. Three different coal seams, lower−middle−upper coal seams, were identified within the Miocene sequences.[29,31] The Soma Formation begins with conglomerates, sandstones, and mudstones at the top and is overlaid by a lower coal seam. The sequence continues with marl deposits toward the top, and limestones overlie the marl levels with increasing carbonate content. The middle coal seam overlying the limestones represents the highest level of the Soma Formation. Sandstone, siltstone, and claystone deposits of the Denis Formation cover this coal seam with an erosional contact. Above these deposits, the Upper coal seam was deposited and overlaid by tuff-marn succession.

The deposits continue with conglomerate, sandstone, and claystone succession toward the top and end with limestone-tuff

https://doi.org/10.1021/acsomega.3c06635
ACS Omega 2023, 8, 47974−47990

Table 1. Result of Rock-Eval Pyrolysis and the Calculated Parameters[a]

well no.	seam	depth/sample ID [m]	lithology	TOC [wt %]	S_1 [mg HC/g rock]	S_2 [mg HC/g rock]	HI [mg HC/g TOC]	BI [mg HC/g TOC]	QI [mg HC/g TOC]	T_{max} [°C]	PI
S332	KP1	412.4	carb. shale	11.7	0.5	5.1	44	5	48	402	0.10
	KP1	417	coal	51.2	1.6	49.8	97	3	100	407	0.03
	KP1	419.4	carb. shale	27.0	1.1	18.7	70	4	74	417	0.05
	KM3	512.3	carb. shale	20.1	0.9	8.6	43	5	48	415	0.10
	KM2	625.6	coal	47.8	1.0	52.5	110	2	112	424	0.02
S338	KP1	518	coal	43.1	1.8	33.3	77	4	81	415	0.05
	KP1	518.9	coal	34.5	1.6	52.2	151	5	156	417	0.03
	KP1	522.9	coal	55.8	1.8	61.2	110	3	113	406	0.03
	KP1	524.3	carb. shale	12.3	2.4	6.6	79	19	73	416	0.26
	KM3	603.7	coal	62.9	1.8	77.7	124	3	126	420	0.02
	KM3	605.2	coal	47.0	0.5	46.2	98	1	99	436	0.01
	KM3	608.4	coal	37.1	1.1	52.0	140	3	143	434	0.02
	KM3	610	coal	57.5	1.2	71.6	125	2	127	430	0.02
S340	KP1	679	coal	31.3	1.2	36.9	118	4	122	434	0.03
	KM2	847.5	coal	50.4	1.6	70.9	141	3	144	423	0.02
	KM2	852.5	coal	61.7	1.6	30.0	49	3	51	420	0.05
	KM2	855	coal	44.2	1.7	19.6	44	4	48	418	0.08
	KM2	858.5	coal	65.7	3.5	52.1	79	5	85	408	0.06
S341	KP1	558	carb. shale	13.2	1.1	1.9	15	8	23	439	0.36
	KM2	724.4	coal	60.0	1.6	38.5	64	3	67	428	0.04
	KM2	730.8	coal	60.4	2.4	46.57	77	4	81	402	0.05
S344A	KM2	770.4	coal	59.6	2.6	76.04	109	4	132	420	0.03
	KM2	784.3	coal	60.8	1.0	77.55	128	2	129	416	0.01
S349B	KM2	783	coal	50.0	2.9	41.57	83	6	89	425	0.06

[a]TOC—total organic carbon, S_1—free hydrocarbons, S_2—hydrocarbons generated during pyrolysis, Tmax—maximum temperature, HI—hydrogen index; HI = $(S_2/TOC) \times 100$, BI—bitumen index; BI = $(S_1/TOC) \times 100$, QI—quality index; QI = $(S_1 + S_2/TOC) \times 100$, PI—production index; PI—$S_1/(S_1 + S_2)$, carb. shale— carbonaceous shale.

succession and andesite, basalt, agglomerate, and tuff overlying them with angular unconformity (Figure 1b). These units are overburdened by Quaternary-aged alluvium and talus.[3,4,29]

3. MATERIALS AND METHODS

Core samples were taken from six drillholes (S332, S338, S340, S341, S344A, and S349B) from different sections of the upper, middle, and lower coal seams (Figure 1a,b). Coals were analyzed by total organic carbon (TOC) and pyrolysis analysis to determine their oil/gas potential prior to complex and detailed chemical analysis. TOC-pyrolysis analysis of 24 rock samples collected from Miocene coals from six drillholes of the Soma-Manisa coal field was performed on a Rock-Eval 6 instrument using the IFP (Institut Francais du Petrolé) standard, and the results were interpreted according to Espitalie et al.,[32] Peters,[33] and Lafargue et al.[34] Seven samples were selected for advanced organic geochemical analyses such as bitumen extraction, thin layer column chromatography, gas chromatography (GC), and Gas chromatography−mass spectrometry (GC-MS). Stable carbon isotope ($\delta^{13}C$) analyses were also performed on these 7 samples. Thin layer chromatography (Iotrascan) was used to determine the samples' saturated, aromatic, polar components, and asphaltene ratios. In this analysis, the MK5 (TLC/FID) thin layer chromatography device "North Sea Oil" standard was used. The extraction process was carried out at ASE 300 with dichloromethane (CH_2Cl) for about 40 h. asphaltene components were removed and separated by column chromatography using a silica−alumina column. At the end of extraction, Agilent 6850 whole-extract GC analysis of saturated hydrocarbon compositions was performed using the ASTM D 5307-97 standard. Agilent 7890A/5975C GC-MS was used to determine the compositional characteristics of the saturated and aromatic compounds sterane (m/z 217) and terpane (m/z 191), monoaromatic (m/z 253), and triaromatic (m/z 231) steroids. Dibenzothiophene, methyldibenzothiophenes, phenanthrene, and methylphenanthrenes were determined from m/z 184, 198, 178, and 192 chromatograms, respectively. Carbon isotope analysis was performed on GV Instruments Isoprime EA-IRMS using the standard $\delta^{13}C_{V\text{-}PDB} = -26.43$ ‰. The results were evaluated according to ‰ (PDB). Huminite reflectance (%, Ro) measurements were made on 23 selected samples, and the maceral distributions were determined. For Ro measurements and maceral analysis, coal samples were ground to a particle size of 1 mm, placed in epoxy resin, and polished. Maceral identification was performed by counting at least 500 points with a Leitz MPV-SP microscope and in accordance with the terminology developed by the International Committee for Coal and Organic Petrology (ICCP) for low-rank coals.[35] Huminite reflectance (Ro, %) was measured according to Taylor et al.[36] (Roil % 0.589), and the results were interpreted in "MPGeor" software. Carbon (C), hydrogen (H), oxygen (O), nitrogen (N), and sulfur (S) contents were analyzed on 23 samples. These analyses were performed according to ASTM (D2013/D2013M, D4239, and D5373) and measured with a LECO analyzer.

Rock-Eval pyrolysis, determination of biomarker distributions, and stable C isotope analysis were carried out at Turkish Petroleum R&D Laboratories; organic petrographic analyses and C, H, O, N, and S elemental analyses were carried out at the MAT Department laboratory of the General Directorate of Mineral Research and Exploration.

https://doi.org/10.1021/acsomega.3c06635
ACS Omega 2023, 8, 47974−47990

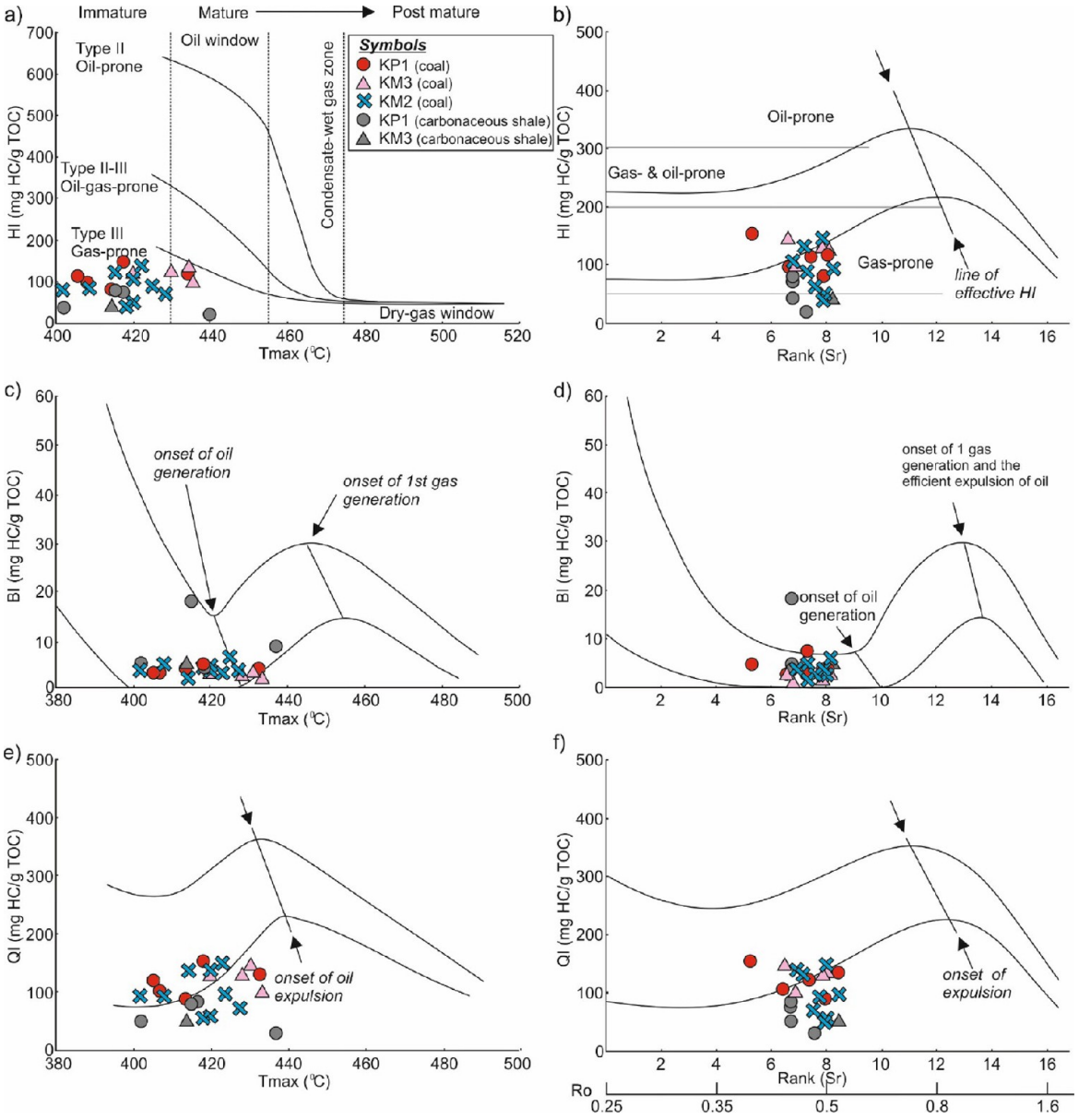

Figure 2. Hydrocarbon generation potential assessment. (a) Plot of HI-Tmax, (b) plot of HI-Ro, (c) plot of BI-Tmax, (d) plot of BI-Ro, (e) plot of QI-Tmax, (f) plot of QI-Ro for Soma-Manisa samples. (adapted with permission from ref 37. Copyright 2023 ACS.,[32,37,38])

4. RESULTS

4.1. TOC and Rock-Eval Parameters. TOC and Rock-Eval pyrolysis results of coal and carbonaceous shale samples of Miocene-aged Denis (KP1 seam) and Soma (KM3 and KM2 seams) Formations are presented in Table 1. The TOC contents of the analyzed samples range from 11.7 to 55.75 wt % in KP1, 20.12−62.86 wt % in KM3, and 50.03−65.71 wt % in KM2. Tmax values are in the range of 402−439 °C in KP1, 415−436 °C in KM3, and 402−428 °C in KM2. Hydrogen index (HI) values in all three seams, except for sample KP1−518.9, show low values and range between 15 and 151 mg HC/g TOC in the KP1 seam, 43 and140 mg HC/g TOC in the KM3 seam, and 44 and141 mg HC/g TOC in the KM2 seam. The HI-Tmax graphs (Figure 2a) also show that the samples reflect values lower than 150 mg HC/g TOC. Quality index (QI) and bitumen index (BI) were calculated for coals and carbonaceous shales (Table 1). BI values ranged from 4 to 19 mg HC/g TOC and 3 to 5 mg HC/g TOC for carbonaceous shale and coal samples in the KP1 seam, from 1 to 5 mg HC/g TOC in the KM3 seam, and from 2 to 8 in the KM2 seam (Figure 2c,d). The QI ranged from 23 to 74 in carbonaceous shale samples in the KP1 seam, 81−156 in coal samples, 48 to 143 in the KM3 seam, and 48−144 in the KM2 seam (Table 1; Figure 2e,f).

4.2. Molecular Composition of Hydrocarbon. *4.2.1. Bulk Geochemical, Isoprenoids, and n-Alkanes.* The amount of EOM varies between 2213 and 3870 ppm, 1626 and 1644 ppm, and 3745 and 9377 ppm in the samples from the KP1, KM3, and KM2 seams, respectively (Table 2). Polar (resin) components predominate in the EOMs of samples from KP1, KM3, and KM2 seams, ranging from 86.51 to 89.48 wt %, 74.41−77.73 wt %, and 71.78−95.43 wt %, respectively. Besides the dominance of polar components, saturated and aromatic components exhibited close percentage distribution. Saturated and aromatic hydrocarbon contents ranged between 7.92 and 8.22 wt %, 2.30 and 5.56 wt % in the KP1 seam; 9.66 and 17.51

https://doi.org/10.1021/acsomega.3c06635
ACS Omega 2023, 8, 47974−47990

Table 2. Extractable Organic Matter (ppm), Percentage of Extract Fractions, and Parameters Calculated from GC for Coal Samples[a]

parameters	sample no.						
	S332 (KP1)	S332 (KM3)	S332 (KM2)	S338 (KP1)	S338 (KM3)	S340 (KP1)	S340 (KM2)
EOM (ppm)	2213	1626	3745	3870	1644	2217	9377
bitum/TOC	0.04	0.08	0.12	0.07	0.03	0.07	0.15
polar (resin (%) + asphaltene (%))	86.77	77.73	95.43	86.51	74.41	89.48	71.78
saturated hydrocarbons (%)	7.92	9.66	3.52	7.93	17.51	8.22	6.22
aromatic hydrocarbons (%)	5.31	12.61	1.05	5.56	8.08	2.30	22.00
Pr/Ph	3.21	2.21	2.14	1.95	5.05	4.67	2.05
Pr/n-C_{17}	1.93	1.40	0.32	1.03	2.42	1.62	2.05
Ph/n-C_{18}	0.66	0.96	0.27	0.62	0.46	0.37	2.43
$CPI_{(24-34)}$[39]	4.27	4.08	3.27	6.22	4.16	4.04	2.92
OEP[40]	2.73	2.41	1.55	2.95	1.58	1.97	1.94
short-chain n-alkanes (n-C_{15-19}) (%)	8.66	11.41	13.23	7.53	7.11	7.95	18.30
middle-chain n-alkanes (n-C_{21-25}) (%)	22.95	28.97	43.89	24.81	35.66	28.60	26.91
long-chain n-alkanes (n-C_{27-31}) (%)	63.56	50.67	30.63	62.79	50.17	56.62	36.82
n-C_{17}/ n-C_{31}	0.10	0.24	0.41	0.13	0.08	0.12	0.56
n-C_{27}/n-C_{31} (Qwood/Qgrass)[41]	0.86	0.85	0.74	1.60	0.58	0.92	0.81
TAR[42]	11.90	6.31	2.99	14.60	9.88	10.13	2.40
Paq[43]	0.28	0.38	0.64	0.33	0.42	0.37	0.45
Pwax[43]	0.78	0.69	0.46	0.76	0.66	0.72	0.64
ACL[44]	29.50	29.57	29.86	28.89	30.23	30.06	29.74
waxiness index	8.82	5.47	4.79	10.07	9.78	9.18	2.25

[a]CPI = 1/2 [(C_{25}+C_{27}+C_{29}+C_{31}+C_{33}/C_{24}+C_{26}+C_{28}+C_{30}+C_{32}) + (C_{25}+C_{27}+C_{29}+C_{31}+C_{33}/C_{26}+C_{28}+C_{30}+C_{32}+C_{34})] (Bray and Evans[39]); OEP = (C_{21}+6C_{23}+C_{25})/(4C_{22}+4C_{24}); TAR = (C_{27}+C_{29}+C_{31})/(C_{15}+C_{17}+C_{19}); Paq = (C_{23}+C_{25})/(C_{23}+C_{25}+C_{29}+C_{31}); Pwax = (C_{27}+C_{29}+C_{31})/(C_{23}+C_{25}+C_{27}+C_{29}+C_{31}); ACL = (27 × C_{27}+29 × C_{29}+31 × C_{31}+33 × C_{33})/(C_{27}+C_{29}+C_{31}+C_{33}); waxiness index = Σ(n-C_{21}−n-C_{31})/Σ(n-C_{15}−n-C_{20}).

wt %, 8.08 and 12.61 wt % in the KM3 seam; and 3.52 and 6.22 wt %, 1.05 and 22.00 wt % in the KM2 seam, respectively.

The relative abundances of n-alkanes in the analyzed samples are listed in Table 2. The identified n-alkane compositions of the coals belonging to the KP1, KM3, and KM2 seams in the Soma basin range from n-C_{10} to n-C_{36} (Figure 3). The studied coal samples are characterized by a high abundance of long-chain (n-C_{27-35}) n-alkanes and a variable proportion of medium-chain (n-C_{21-25}) and short-chain (n-C_{15-19}) n-alkanes. The predominance of significant n-alkanes longer than C_{27} and the distributions accompanied by n-C_{25} alkane peaks indicate occasional mixing of organic matter sources. It also exhibits a unimodal distribution toward long-chain n-alkanes. Diffractomes of Soma coals show the presence of a small unresolved complex mixture (UCM) indicating bacterial activity. The Pr/Ph ratio presented high (>1) values. The carbon preference index (CPI) was high in all samples, ranging from 4.04 to 6.22 (avg. 4.84) in KP1, 4.08 and 4.16 (avg. 4.12) in KM3, and 2.92 and 3.27 (avg. 3.1) in KM2 (Table 2).

4.2.2. Terpanes and Steranes. The terpane distribution of Soma-Manisa coal samples (m/z 191) is characterized by the relative dominance of $C_{30}17\alpha$, 21β (H)-hopane, C_{30} tricyclic terpane, and C_{29} 17α, 21β (H)-30-norhopane and homomoretane (Figure 4). As shown in Table 3, the Ts/Tm ratio is extremely low in the study area, ranging between 0.03 and 0.20. The 22S/(22S+22R) (C_{32}) homohopane isomerization ratios of the analyzed samples are in the range 0.08−0.21 and have not reached equilibrium. In all samples, C_{31} homohopane is more dominant than C_{32} homohopane and the C_{35}/C_{31}−C_{35} homohopane ratio presented very low values. In addition, the gammacerane index (G/C_{30} H),[45] which provides information on the salinity level of the depositional environment, is extremely low (<0.14) in all source rock extracts (Table 3).

In the m/z 217 saturated hydrocarbon fragmantogram represented by the GC-MS chromatogram of the studied samples, the dominance of regular steranes over diastereosteranes as well as the dominance of C_{29} and C_{28} steranes shows variations (Figure 4 and Table 3). The $\beta\beta/(\beta\beta+\alpha\alpha)$ sterane ratio increases as the depth increases from the upper seam (KP1) to the lower seam (KM2) (Table 3).

4.2.3. Aromatic Hydrocarbons and Polar Compounds. The distributions of monoaromatic (MA) and triaromatic (TA) steroids among aromatic hydrocarbons were obtained from mass chromatograms at m/z 253 and m/z 231, respectively; the distributions of phenanthrenes and dibenzothiophenes among polycyclic aromatic hydrocarbons and their alkyl derivatives were obtained from mass chromatograms at m/z 178, 192 and m/z 184, 198, respectively (Figure 5). The C_{27}−C_{28}−C_{29} MA steroid distribution in all samples of Soma-Manisa coals was determined as C_{29} > C_{28} > C_{27} (Table 4). The $C_{29}/(C_{29}+C_{28})$ MA steroid ratio gave an average value of 0.8 in the coals of the studied seams. The Dia/(Dia+R) MA ratio was determined in the range of 0.50−0.79 (Table 4). The MA(I)/MA(I+II) ratio was calculated as <0.1 in the KP1, KM3, and KM2 seams. The parameters calculated from phenanthrene (P) and methylphenanthrene (MP) distributions in coal samples are given in Table 4. Phenanthrene is more dominant than methylphenanthrene (Figure 5c). Methylphenanthrene index-1* (MPI-1*) values are in the range of 0.58−0.85. In addition, the order MPR-9 > MPR-2 > MPR-1 > MPR-3 is generally dominant in the samples. Methyldibenzothiophene ratio (MDR and MDR′) values are found at similar abundances in coal samples (Table 4). Low dibenzothiophene (DBT) concentrations (S338—605.20; except for KM3) have been detected in samples from KP1, KM3, and KM2 seams. DBT/P ratios of these coal samples range between 0.29 and 1.02 (Table 4).

https://doi.org/10.1021/acsomega.3c06635
ACS Omega 2023, 8, 47974−47990

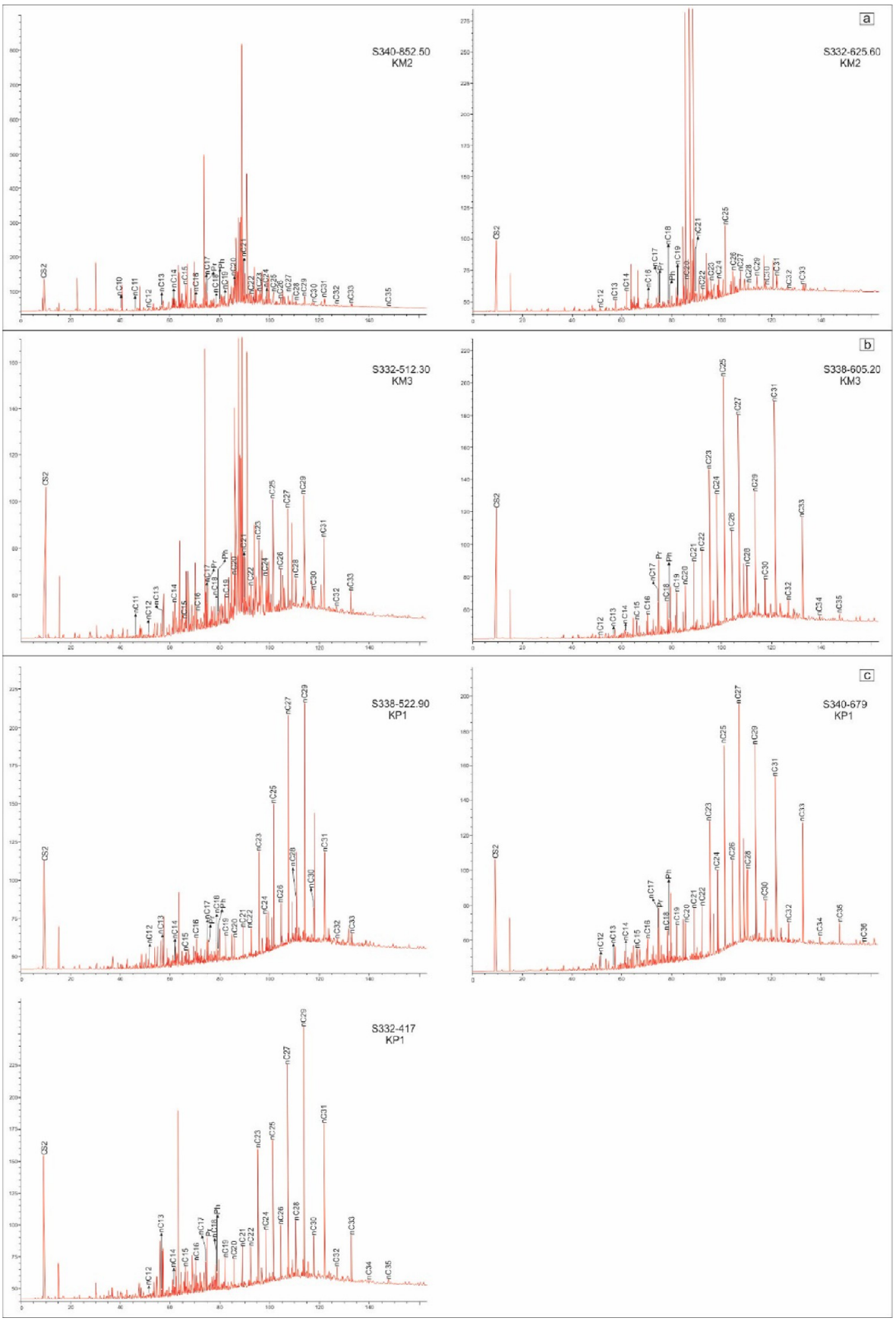

Figure 3. *n*-Alkane and isoprenoid distribution of (a) KM2, (b) KM3, and (c) KP1 samples.

https://doi.org/10.1021/acsomega.3c06635
ACS Omega 2023, 8, 47974−47990

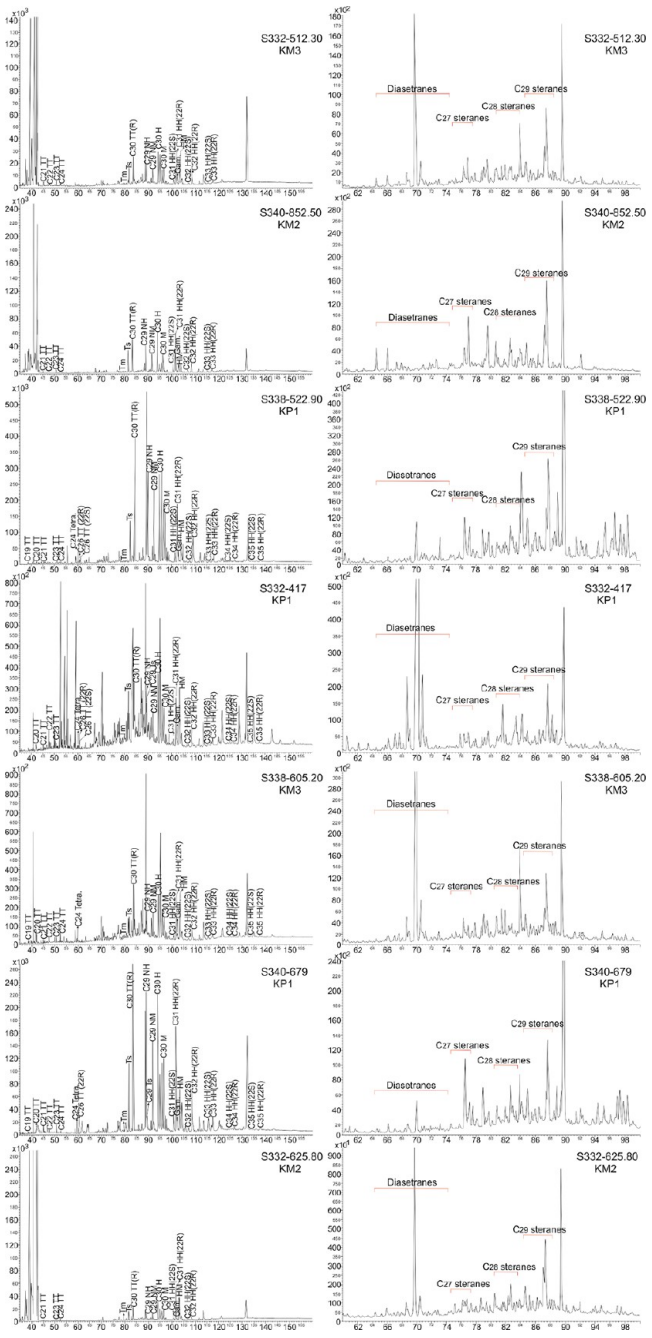

Figure 4. Representative saturated hydrocarbon m/z 191 and m/z 217 chromatograms showing terpane and sterane distributions in the coals. Abbreviations: TT = tricyclic terpane; Ts = 18$\alpha(H)$-trisnorneohopane; H = hopane; Gam. = gammacerane; Tm = 17$\alpha(H)$-trisnorhopane; C_{29} H = 30-norhopane; C_{30}H = 17$\alpha(H)$. 21$\beta(H)$-hopane; C_{27} to C_{29} = C_{27} to C_{29} regular steranes.

4.3. Stable C Isotope and Elemental Compositions. The stable carbon isotope (δ^{13}C, ‰ (VPDB)) results of Deniş (KP1 seam) and Soma (KM3 and KM2 seams) Formation coals are shown in Table 5. The δ^{13}C values of the KP1 seam ranged between −27.48 and −27.25‰ (avg. −27.39‰), the δ^{13}C values of the KM3 seam ranged between −27.52 and −25.68‰ (avg. −26.6‰), and the δ^{13}C value of the KM2 seam was −24.97‰. In addition, the saturated hydrocarbon ($\delta^{13}C_{Sat.}$) and aromatic hydrocarbon ($\delta^{13}C_{Aro}$) fractions of bitumen extracts are listed in Table 5. In the KP1, KM3, and KM2 seams, the average $\delta^{13}C_{Sat}$ values are −28.74, −27.84, and −26.41‰ while the average $\delta^{13}C_{Aro}$ values are −27.76, −27.53, and −25.87‰, respectively. In all seams, the chief distribution was determined as $\delta^{13}C_{Aro} > \delta^{13}C_{Sat.}$

Table 5 lists the results of the elemental analysis of the analyzed coal samples. The total sulfur contents of the coal samples on a dry basis were determined to be 2.54−8.33% (avg. 5.83%), 0.54−12.35% (avg. 4.68%), and 0.14−4.14% (avg. 2.54%) in the KP1, KM3, and KM2 seams, respectively. C (10.16−50.51%), H (1.40−3.45%), N (0.29−1.06%), and O (36.65−85.61%) on a dry basis in the KP1 seam; C (15.78−47.04%), H (0.82−3.37%), N (0.24−1. 31), and O (35.93−82.62%) on a dry basis in the KM3 seam; and C (18.25−71.01%), H (1.24−4.72%), N (0.27−1.33%), and O (22.42−80.1%) on a dry basis in the KM2 seam show a wide distribution. The H/C and O/C ratios of the coals in the Deniş and Soma Formations were also calculated (Table 5). In the KP1 seam in the Denis Formation, H/C ratios are between 0.07 and 0.14 (avg. 0.09) and O/C ratios are between 0.73 and 8.43 (avg. 3.05). In the KM3 seam in the Soma Formation, H/C ratios range between 0.05 and 0.08 (avg. 0.07) and O/C ratios range between 0.76 and 5.24 (avg. 2.10); in the KM2 seam, H/C ratios range between 0.06 and 0.08 (avg. 0.07) and O/C ratios range between 0.32 and 4.39 (avg. 1.18). The H/C ratios of the coals in the KP1 seam are higher than the H/C ratios of the coals in the KM3 and KM2 seams. The C/N ratios of the samples ranged between 31.90 and 55.96 (avg. 44.19) in the KP1 seam, 35.91−65.75 (avg. 46.98) in the KM3 seam, and 43.19−161.39 (avg. 82.66) in the KM2 seam and presented high values (>10).

4.4. Maceral Distributions. Organic petrographic observations indicate higher amounts of huminite/vitrinite compared to liptinite and inertinite macerals in each of the three seams in the Soma-Manisa basin. The average huminite macerals are 53.78, 54.75, and 67.89% in coal samples from the KP1, KM3, and KM2 seams, respectively. Organic petrographic studies revealed abundance of texinite, ulminite, atrinite, densinite, corpohuminite, and gelinite (huminite group macerals) and lower amounts of sporinite, cutinite, and resinite (liptinite group macerals) and fusinite, funginite, macrinite, and inertodetrinite (inertinite group macerals) (Table 6 and Figure 6). In the KP1, KM3, and KM2 seams, the Gelification Index (GI) calculated from maceral compositions ranged between 1.3 and 3.6, between 1.1 and 1.5, and between 1.3 and 2.5; the Tissue Preservation Index (TPI) ranged between 0.5 and 1.2, between 0.5 and 0.6, and between 0.8 and 2. 8; the Groundwater Index (GWI) ranged between 1.1 and 4.1, between 1.2 and 2.5, and between 0.5 and 2; and the Vegetation Index (VI) ranged between 0.6 and 2.1, between 0.5 and 0.8, and between 0.9 and 4.5, respectively (Table 6).

5. DISCUSSION

5.1. Type, Origin of Organic Matter, and Depositional Environments. According to TOC (wt %) values, the studied samples, which have excellent source rock potential, contain type III kerogen. Considering the HI-Tmax diagram[49,50] and effective HI values in the HI-Ro diagram,[38,51,52] coals of the KP1, KM3, and KM2 seams have gas-prone potential (Table 1 and Figure 2a,b). Low Production Index (PI) (<0.10), BI (<8), and QI (<144) values and HI-Ro, BI-Ro, BI-Tmax, QI-Ro, and QI-Tmax diagrams support that the three seams are essentially gas-prone (Table 1 and Figure 2c−f).

Nitrogen values range from 0.29 to 1.06 wt % in the KP1 seam, 0.24 to 1.31 wt % in the KM3 seam, and 0.27 to 1.33 wt % in the

https://doi.org/10.1021/acsomega.3c06635
ACS Omega 2023, 8, 47974−47990

Table 3. Parameters Calculated from Saturated Biomarker Distributions (m/z 191 and m/z 217 Mass Chromatograms) for Soma-Manisa Coals

	S332 (KP1)	S332 (KM3)	S332 (KM2)	S338 (KP1)	S338 (KM3)	S340 (KP1)	S340 (KM2)
Terpanes							
C_{29}/C_{30} hopane	0.49	0.56	0.33	0.98	0.58	0.98	0.67
Ts/Tm	0.13	0.12	0.08	0.04	0.20	0.03	0.06
Ts/(Ts + Tm)	0.11	0.11	0.08	0.04	0.17	0.03	0.06
moretane/hopane	0.51	0.45	0.54	0.55	0.48	0.52	0.42
C_{23} TT/(C_{23} TT + C_{30} H)	0.08	0.16	0.07	0.02	0.12	0.06	0.07
C_{35}/(C_{31} − C_{35}) homohopane	0.03	0	0	0.02	0.04	0.02	0
22S/(22S+22R) (C_{32})	0.12	0.19	0.26	0.08	0.12	0.09	0.21
Gam/C_{30} H	0.12	0.08	0.08	0.11	0.14	0.10	0.05
Steranes							
diasterane/sterane	2.88	1.79	0.90	0.61	1.29	0.28	5.21
C_{27} sterane (%)	6.05	10.04	12.17	5.81	9.61	18.37	6.76
C_{28} sterane (%)	58.12	47.23	31.54	34.26	52.48	30.05	37.21
C_{29} sterane (%)	35.83	42.73	56.28	59.93	37.91	51.58	56.03
iso-sterane (%)	7.41	14.68	15.64	25.91	13.65	24.50	20.74
n-sterane (%)	4.77	14.37	18.30	40.92	11.14	44.71	38.73
dia-sterane (%)	87.82	70.95	66.06	33.18	75.21	30.79	40.53
$\beta\beta/(\beta\beta+\alpha\alpha)$	0.36	0.42	0.44	0.35	0.40	0.38	0.38
sterane/17αH	0.20	0.12	0.09	0.04	0.28	0.02	0.08

KM2 seam, averaging 0.66, 0.83, and 0.71 wt %, respectively. The TOC/N ratio is widely used to distinguish between vascular plants and planktonic/algal material.[53,54] TOC/N ratios are greater than 15 for vascular plants, between 4 and 10 for aquatic plants, and between 6 and 9 for planktonic/algal material.[53] The nitrogen content of organic matter in terrestrial vegetation and surrounding marsh sediment is generally low.[24,54] TOC/N ratios are >15 in the samples from three seams. Similarly, C/N ratios are also high, indicating high terrestrial vegetation.[55] Stable carbon isotopic ($\delta^{13}C$) values are an important tool used to determine the origin and differentiation of organic matter between different depositional environments, either marine or terrestrial.[56−59] The $\delta^{13}C$ values of the samples of the KP1, KM3, and KM2 seam were between −24.97 and −27.52‰ (Table 5), indicating that they are compatible with the material between the terrestrial C_3 type vegetation and the coal seen in Figure 7a. When C/N and $\delta^{13}C$ are evaluated together (Figure 7b), it can be concluded that Soma-Manisa coals have the same origin and originated from a terrestrial source.[60]

Polars and asphaltenes (between 71.78 and 89.48%) constituted the majority of the soluble organic matter in Soma-Manisa coals (Table 2). This indicates the input of terrestrial plants and low maturity.[62]

Short-chain *n*-alkanes are common in algae/microorganisms.[63] *N*-C_{16}, *n*-C_{17}, and *n*-C_{19} alkanes are abundant in the samples of the KP1 seam; *n*-C_{17} and *n*-C_{19} are abundant in the samples of the KM3 and KM2 seams (Figure 3). The samples of the upper seam (KP1) have a much higher *n*-C_{16} peak than other short-chain homologues. The presence of a small amount of UCM in the area of short-chain *n*-alkanes in the diffractome indicates bacterial activity.[64−66] The *n*-C_{20} and *n*-C_{25} homologues of medium-chain alkanes are relatively enriched. The abundances of C_{23} and C_{25} *n*-alkanes originate from Sphagnum[67−70] and/or aquatic macrophytes (macroscopic algae) in swamp environments.[43,68,71] The Paq and Pwax parameters, which are used especially for coals, can be calculated to obtain information about the plant species in the environment from which the organic matter derived and thus about the paleoclimatic conditions of the environment.[41] The Paq ratio is used to estimate the ratio of submerged or aquatic plants to terrestrial and emergent plant input.[43] The *n*-alkanes C_{23} and C_{25} are common in submerged and floating plants, while C_{29} and C_{31} are typically common in terrestrial plants. Paq <0.1 reflects terrestrial plant input, Paq values in the range 0.1−0.4 reflect emergent plant, and Paq values in the range 0.4−1 reflect submerged/floating plants (macrophytes, aquatic land (peat) mosses, aquatic ferns, seed plants). Paq values were calculated as 0.28−0.37 (avg 0.33) in samples from the KP1 seam, 0.38−0.42 (avg 0.40) in samples from the KM3 seam, and 0.45 and 0.64 (avg 0.55) in samples from the KM2 seam (Table 2). The Paq values of KP1 and KM3 seams indicate a submerged plant input, whereas the Paq value of the KM2 seam indicates a submerged/floating plant input. The Pwax value reflects the relative ratio of waxy hydrocarbons derived from floating plants and terrestrial plants to total hydrocarbons.[41] A Pwax value >0.7 indicates dry climate conditions, while <0.7 indicates humid climate conditions. In the KP1, KM3, and KM2 seams, Pwax values are between 0.72 and 0.78, between 0.66 and 0.69, and between 0.46 and 0.64, respectively. As the depth increased, there was a transition from dry to humid climate.

Long-chain *n*-alkanes, dominated by *n*-C_{27} and *n*-C_{29} alkanes, are characteristic of waxy woody plants.[71,72] The distributions of *n*-C_{29} and *n*-C_{31} alkane abundances are similar due to epicuticular waxes in both terrestrial and emergent plants.[43,68,72,73] For this reason, long-chain *n*-alkanes, in which odd-numbered carbon predominates over even-numbered carbon (such as *n*-C_{27} or *n*-C_{29} and *n*-C_{31}) in the studied coal samples, indicate an important contribution of aquatic emergent/terrestrial plant input.

The high CPI values observed in the samples from seams KP1, KM3, and KM2 (Table 2) indicate terrestrial plants and a low degree of maturity due to the long-chain *n*-alkane content of the coals.[20,74]

The average chain length (ACL) index shows the concentration-weighted ACL of C_{27}−C_{33} *n*-alkanes and can indicate local temperature variation[75] as well as different vegetation types.[44,76,77] Plants in cold/dry areas have higher values than in warm/humid areas.[44] In other words, a high ACL

https://doi.org/10.1021/acsomega.3c06635
ACS Omega 2023, 8, 47974−47990

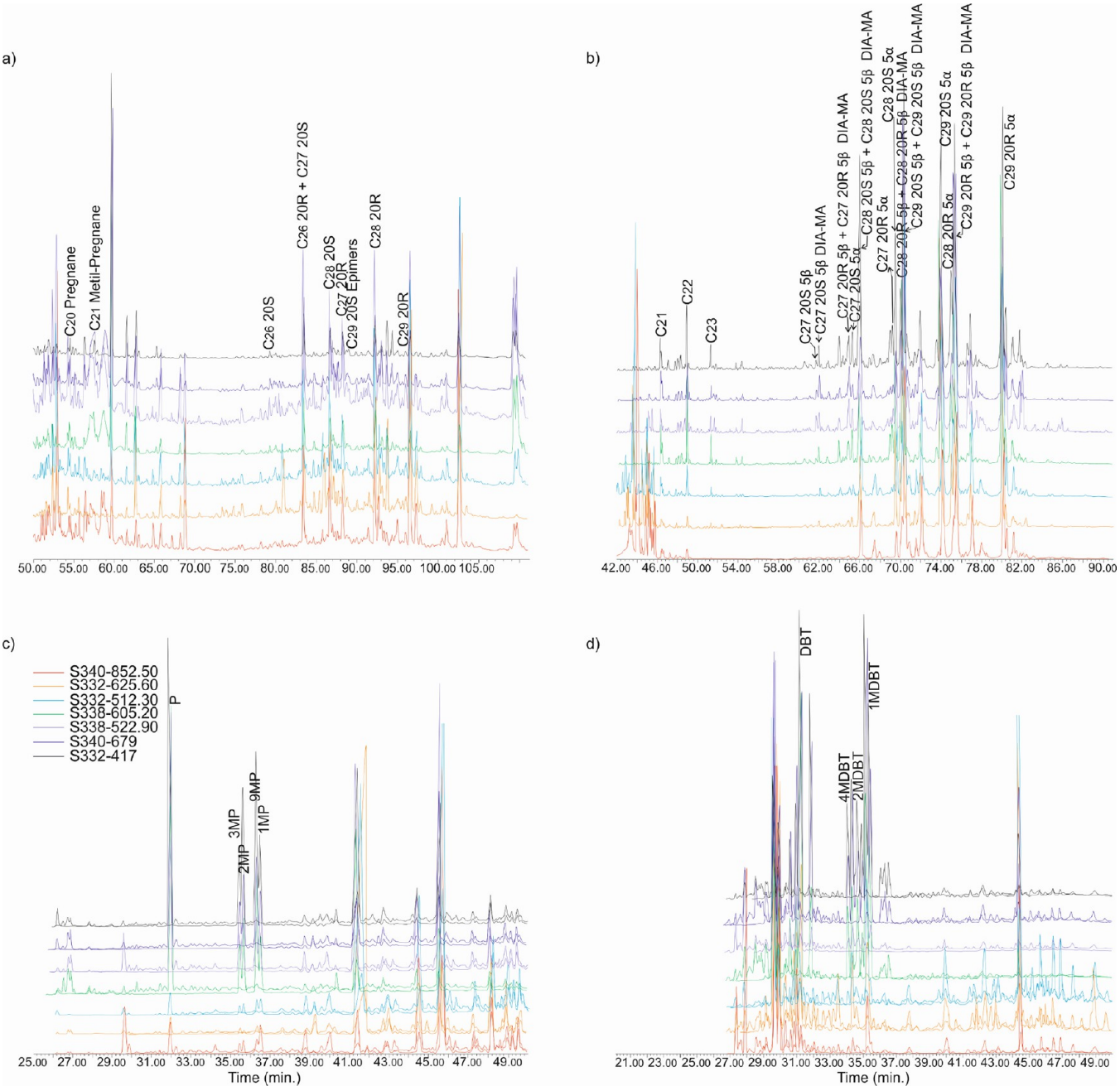

Figure 5. (a) m/z 231 mass fragmentograms, (b) m/z 253 mass fragmentograms, (c) m/z 178 + 192 mass fragmentograms, and (d) m/z 184 + 198 mass fragmentograms of aromatic hydrocarbons for Soma-Manisa coal samples. P—phenanthrene, MP—methylphenanthrene, DBT—dibenzothiophene, MDBT—methyldibenzothiophene.

index value indicates dry and cold climatic conditions with vascularized plants. It was determined as 28.89−30.06 in the samples taken from the KP1 seam, 29.57−30.23 in the samples taken from the KM3 seam, and 29.74−29.86 in the samples taken from the KM2 seam. The decrease/change in the ACL index with some fluctuation from the lower to the upper seam indicates that the organic matter has changed from humid and rainy climatic conditions to moderately humid climatic conditions and may be derived from vascular plants.

Pr/Ph ratios are used to describe oxic/anoxic depositional conditions.[20,78−80] In general, low Pr/Ph ratios (<1) indicate anoxic conditions for the accumulation of organic matter from land plants, while high Pr/Ph ratios (>3) indicate oxic conditions and Pr/Ph ratios between 1 and 3 indicate suboxic conditions.[74,78] The Pr/Ph ratio in the coal samples examined presented high (>1) values. A high Pr/Ph ratio indicates suboxic−oxic conditions in the depositional environment and the contribution of vascular plants. This ratio usually gives values greater than 1 due to the high TOC content in coals[17,81−83] and indicates the input of oxidized terrestrial plant material to swamps.[24] These values are supported by the Pr/nC$_{17}$−Ph/nC$_{18}$ diagram (Figure 8).

In the nC$_{17}$/nC$_{31}$ ratio of the lower, middle, and upper coal seams (0.41−0.56 for KM2, 0.08−0.24 for KM3, and 0.10−0.13 for KP1), the analyzed samples contain organic matter originating from terrestrial plants as nC$_{31}$ n-alkanes are more dominant[84] (Table 2). Another parameter used to determine the type of organic matter of terrestrial origin is the Waxiness index.

https://doi.org/10.1021/acsomega.3c06635
ACS Omega 2023, 8, 47974−47990

Table 4. Parameters Calculated from Aromatic Biomarker Distributions (m/z 231, 253, 178, 192, 187, and 198 mass chromatograms) for Soma-Manisa Coal Units[a]

	S332 (KP1)	S332 (KM3)	S332 (KM2)	S338 (KP1)	S338 (KM3)	S340 (KP1)	S340 (KM2)
Steroid							
TA(I)/TA(I + II)	0.20	0.08	0.07	0.15	0.28	0.22	0.12
MA(I)/MA(I + II)	0.05	0.04	0.02	0.05	0.09	0.06	0.03
C_{27} MA steroid (%)	8.11	3.21	2.60	8.75	8.78	8.57	1.11
C_{28} MA steroid (%)	30.21	22.65	24.61	18.85	23.27	20.23	22.76
C_{29} MA steroid (%)	61.68	74.14	72.78	72.40	67.96	71.19	76.13
Dia/(Dia + R) MA	0.73	0.79	0.76	0.54	0.76	0.72	0.50
$C_{29}/(C_{28} + C_{29})$ MA	0.7	0.8	0.7	0.8	0.7	0.8	0.8
Phenantrane							
MPR	1.50	0.69	0.67	1.06	1.33	1.30	0.47
MPR-1	0.32	0.72	0.33	0.35	0.20	0.25	0.93
MPR-2	0.48	0.50	0.22	0.38	0.27	0.33	0.44
MPR-3	0.24	0.42	0.35	0.28	0.18	0.21	0.38
MPR-9	0.61	0.74	0.44	0.41	0.43	0.41	0.49
MPI-1	0.56	0.56	0.49	0.56	0.40	0.48	0.51
MPI-1*	0.78	0.63	0.75	0.85	0.70	0.80	0.58
Dibenzothiophene							
MDR	0.49	0.53	nd	0.49	0.56	0.46	0.62
DBT/P	0.95	0.29	0.56	0.42	1.02	0.53	0.70

[a]TA(I)/TA(I + II) = $(C_{20} + C_{21})/(C_{20} + C_{21} + C_{26} + C_{27} + C_{28})$; MA(I)/MA (I + II) = $(C_{21} + C_{22})/(C_{21} + C_{22} + C_{27} + C_{28} + C_{29})$; MPI-1 = 1.5*(2-MP + 3-MP)/(P + 9-MP + 1-MP); MPI-1*= (2-MP + 3-MP)/(1-MP + 9-MP); MDR= 4-MDBT/1-MDBT; nd: not detected.

Table 5. ^{13}C (‰) Stable Isotope and and H, C, N, O, and S Elemental (%, Dry Basis) Contents of the Analyzed Samples

well no.	seam	depth (m) sample ID	C	H	O	N	S	H/C	O/C	C/N	TOC/S	TOC/N	$\delta^{13}C_{bulk}$ (‰ vs VPDB)	$\delta^{13}C_{saturated}$ (‰ vs VPDB)	$\delta^{13}C_{aromatic}$ (‰ vs VPDB)
S332	KP1	412.4	13.44	1.56	80.07	0.37	4.56	0.12	5.96	36.32	2.57	31.62			
	KP1	417	39.04	2.92	48.95	0.81	8.28	0.07	1.25	48.20	6.18	63.21	−27.43	−28.27	−27.47
	KP1	419.4	15.31	1.74	78.63	0.48	3.84	0.11	0.00	31.90	7.03	56.25			
	KM3	512.3	15.78	0.82	82.62	0.24	0.54	0.05	5.24	65.75	37.22	83.75	−25.68	−26.87	−26.36
	KM2	625.6											−24.97	−26.04	−25.38
S338	KP1	518	35.97	2.79	52.56	0.7	7.98	0.08	1.46	51.39	5.40	61.57			
	KP1	518.9	38.05	2.63	52.64	0.68	6	0.07	1.38	55.96	5.75	50.74			
	KP1	522.9	38.63	2.91	49.88	0.78	7.8	0.08	1.29	49.53	7.15	71.54	−27.25	−29.59	−27.28
	KP1	524.3	10.16	1.4	85.61	0.29	2.54	0.14	8.43	35.03	3.27	28.67			
	KM3	603.7	47.04	3.37	35.93	1.31	12.35	0.07	0.76	35.91	5.09	48.02			
	KM3	605.2	29.21	2.46	64.45	0.72	3.16	0.08	2.21	40.57	14.87	65.28	−27.52	−28.81	−28.7
	KM3	608.4	44.98	3.23	47.22	1	3.57	0.07	1.05	44.98	10.39	37.10			
	KM3	610	41	2.52	51.84	0.86	3.78	0.06	1.26	47.67	15.21	66.86			
S340	KP1	679	32.96	2.19	60.96	0.79	3.1	0.07	1.85	41.72	10.10	39.62	−27.48	−28.36	−28.52
	KM2	847.5	62.37	4.29	28.36	1.33	3.65	0.07	0.45	46.89	13.81	37.89			
	KM2	852.5	48.49	3.16	44.37	0.65	3.33	0.07	0.92	74.60	18.53	94.92	−25.29	−26.41	−25.87
	KM2	855	71.01	4.72	22.42	0.44	1.41	0.07	0.32	161.39	31.35	100.45			
	KM2	858.5	42.46	2.96	50.87	0.44	3.27	0.07	1.20	96.50	20.09	149.32			
S344A	KM2	770.4	18.25	1.24	80.1	0.27	0.14	0.07	4.39	67.59	52.28	220.74			
	KM2	784.3	55.72	3.69	37.1	1.29	2.2	0.07	0.67	43.19	27.64	47.13			
S349B	KM2	783	35.51	2.68	60.01	0.48	1.32	0.08	1.69	73.98	37.88	104.17			
S341	KP1	558	50.51	3.45	36.65	1.06	8.33	0.07	0.73	47.65	1.58	12.45			
	KM2	724.4	61.73	4.03	29.86	1	3.38	0.07	0.48	61.73	17.75	60.00			
	KM2	725.6	60.23	3.52	31.6	0.51	4.14	0.06	0.52	118.10	14.59	118.43			

The Waxiness index was calculated between 8.82 and 10.07 in the KP1 seam, 5.47−9.78 in the KM3 seam, and 2.14−4.79 in the KM2 seam, indicating a terrestrial input with mainly higher plants.[72,74,84] In addition, high-concentration n-C_{27}/n-C_{31} ratios can be used to assess the relative contribution of the plant species from which the organic matter is derived—shrubs and trees and/or herbaceous plants.[43] It was calculated as 0.86−1.60 in the KP1 seam; 0.58−0.85 in the KM3 seam; and 0.74−0.81 in the KM2 seam (Table 2). These values are characterized by organic matter derived from environments with woody plants.

The sterane/17$\alpha(H)$-hopane ratio reflects prokaryotic versus eukaryotic input.[20,74] Thus, the sterane/17$\alpha(H)$-hopane ratio is relatively high in marine organic matter. In contrast, low sterane and sterane/hopane ratios are indicative of terrestrial and/or microbiologically reworked organic matter.[20] Very low sterane/hopane ratios (<0.5) are caused by aerobic bacteria.[20,85] In this

https://doi.org/10.1021/acsomega.3c06635
ACS Omega 2023, 8, 47974−47990

Table 6. Huminite Reflection (%Ro) Values and Maceral Distributions of the Studied Samples[a]

	Ro	T	U	A	D	Ch	G	ΣH	Sp	Cu	Rs	ΣL	Fs	Fg	M	Id	ΣI	MM	GI	TPI	GWI.	VI
sample ID	[%]	[vol %]																				
S338-518 (KP1)	0.36	4	17	16	17	4	6	64	2	1		3		2	4	2	8	25	1.6	0.6	1.4	0.6
S338-518.9 (KP1)	0.37	2	18	15	10	5	8	58	3	1	2	6	2	2	5	2	11	25	1.5	0.8	1.4	0.9
S338-522.9 (KP1)	0.37	3	19	17	14	3	9	65	2	1	1	4	1	2	3	3	9	22	1.6	0.6	1.2	0.7
S338-524.3 (KP1)	0.36	2	11	10	9	2	6	40	1	1		2		1	3	2	6	52	1.6	0.6	3	0.7
S338-603.7 (KM3)	0.45	3	13	11	10	2	9	48	2	1	2	5	1	1	4	3	9	38	1.5	0.6	2.2	0.8
S338-605.2 (KM3)	0.44	3	10	13	10	2	7	45	1	1	1	3	2		2	1	5	47	1.4	0.6	2.5	0.7
S338-608.4 (KM3)	0.44	2	15	19	16	7	7	66	2	2	2	6	2	1	7	4	14	14	1.3	0.6	1.2	0.6
S338-610 (KM3)	0.46	1	13	18	16	5	7	60	2	1	2	5	2	1	8	6	17	18	1.1	0.5	1.4	0.5
S332-412.4 (KP1)	0.37	1	15	3	2	1	7	29	1			1			1	2	3	67	3.6	1.2	4.1	2.1
S332-417 (KP1)	0.37		18	8	6	3	8	43	1			1		1	1	1	3	53	3.2	0.9	2.7	1.2
S332-419.4 (KP1)	0.38	3	25	7	6	2	12	55	1	1		2		1	2	2	5	38	3	1.1	1.7	1.8
S332-512.3 (KM3)	0.46																					
S332-625.6 (KM2)	0.45	9	31	16	9	6	7	78	1	1	2	4		1	3	2	6	12	1.7	1.4	0.6	1.5
S340-679 (KP1)	0.37	3	18	21	17	3	6	68	1	1	2	4	1	1	2	2	6	22	1.5	0.5	1.1	0.6
S340-847.5 (KM2)	0.48	13	19	2	17	3	6	62	1	1	1	3	1	1	7	3	12	23	1.7	1.2	1.5	1.5
S340-852.5 (KM2)	0.49	11	16	2	16	4	8	59	1	1	2	4	1	1	5	2	9	28	2.1	1	2	1.2
S340-855 (KM2)	0.49	11	30	6	12	6	9	74	1	1	3	5		1	2	3	6	15	2.5	1.6	0.9	2
S340-858.5 (KM2)	0.50	10	38	7	10		12	77			10	10			7		7	6	2.4	1.6	0.5	3.2
S344A-770.4 (KM2)	0.46	14	36	7	5	3	6	71			8	8			4		4	17	1.9	2.8	0.5	4.5
S344A-784.3 (KM2)	0.47	12	26	8	6	3	6	61	1		3	4			4	2	6	29	1.6	1.9	2	2.5
S349B-783 (KM2)	0.49	11	20	12	10	3	7	63	1		3	4			3	2	5	28	1.4	1.1	1.1	1.4
S341-558 (KP1)	0.37	2	16	20	16	4	4	62	2	1	3	6		1	4	4	9	23	1.3	0.5	1.2	1.6
S341-724.4 (KM2)	0.48	10	17	15	13	3	8	66	2		2	4			3	3	6	24	1.3	0.8	1.1	0.9

[a]T—textinite, U—ulminite, A—attrinite, D—densinite, Ch—corpohuminite, G—gelinite, Sp—sporinite, Cu—cutinite, Rs—resinite, Fs—fusinite, Fg—funginite, M—macrinite, Id—inertodetrinite, MM—mineral matter, GI—Gelification Index: (ulminite + gelinite + corpohuminite + densinite)/(textinite + attrinite + inertinite), TPI—Tissue Preservation Index: (textinite + ulminite + corpohuminite + fusinite)/(attrinite + densinite + gelinite + inertodetrinite), GWI—Ground Water Index: (corpohuminite + gelinite + mineral matter + densinite)/(textinite + ulminite + attrinite), VI—Vegetation Index: (textinite + ulminite + resinite + suberinite + fusinite + semifusinite + sporinite + cutinite)/(densinite + attrinite + cutinite + sporinite + algnite + bituminite + inertodetrinite + liptodetrinite) (calculations from Calder et al.[46], Diessel,[47] and Kalkreuth et al.[48]).

study, the high contribution of terrestrial organic matter but significantly low sterane/hopane ratios (Table 3) indicate a high activity of aerobic bacteria, which is consistent with the presence of UCM (Figure 3). High C_{29} and C_{30} hopane values in coal are usually due to aerobic/anaerobic bacterial degradation of terrestrial vegetation.[80,86] The relative dominance of C_{30} 17α(H)-hopane, the most abundant terpane, followed by C_{30} tricyclic terpane, C_{29} 17α(H)-norhopane, and homomoretane in the analyzed samples, indicate bacterial contribution (Figure 4). The distribution of C_{31-35} homohopanes can be used to interpret redox conditions.[20] The predominance of C_{31} and C_{32} homohopanes and low C_{35}/C_{31-35} homohopanes in coals indicates a suboxic and/or oxic environment. In addition, the decrease from C_{31} homohopane to C_{35} homohopane (Figure 4) and the low C_{29}/C_{30} hopane ratio (<1) (Table 3) indicate paleoprecipitation in a clastic environment.[87] Moreover, the Dia/(Dia+R) MA ratios (Table 4) support the presence of coals rich in clastic material dominated by terrestrial organic contribution.[20] 4-MDBT > 2 + 3-MDBT > 1-MDBT was detected in all analyzed samples (Figure 5d). The fact that it

https://doi.org/10.1021/acsomega.3c06635
ACS Omega 2023, 8, 47974−47990

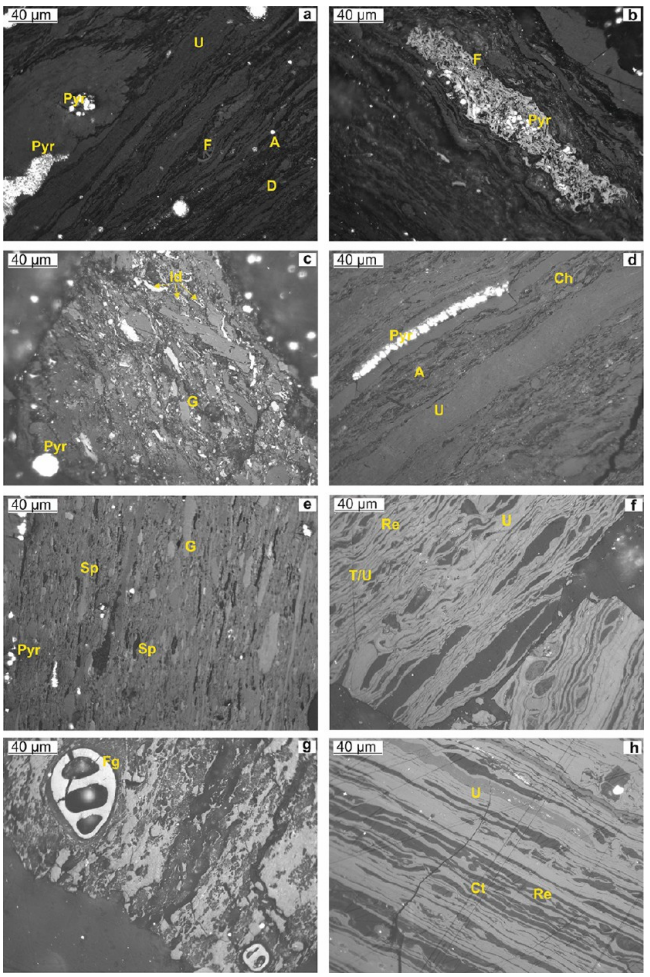

Figure 6. Some photomicrographs of the macerals in the Soma-Manisa coals (KP1—upper seam, KM3—middle seam, and KM2—lower seam). Samples are KP1 (a, b, c), KM3 (d, e), and KM2 (f, g, h). T—textinite, U—ulminite, A—attrinite, D—densinite, G—gelinite, Ch—corpohuminite, S—sporinite, Re—resinite, Cu—cutinite, Fg—fungin-ite, F—fusinite, Id—inertodetrinite, and Pyr—pyrite.

presents a stepwise pattern is predominantly associated with siliciclastic source rocks.[88]

The widely used C_{27}−C_{28}−C_{29} sterane distributions, which vary depending on the type of organic matter, provide information about the paleoenvironment.[20] In the relative variable dominance of C_{29} and C_{28} steranes in the samples

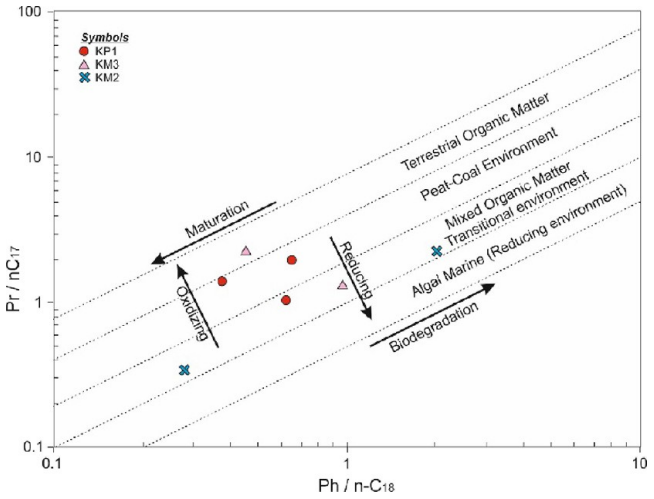

Figure 8. Ph/n-C_{18} versus Pr/n-C_{17} in the Soma-Manisa coal samples.

analyzed (Table 3), the dominance of C_{29} steranes indicates a dominant source of organic matter from vascular plants while the dominance of C_{28} steranes indicates the presence of lacustrine algae.[20,87] Moreover, the triangular diagram of C_{27}−C_{28}−C_{29} steranes shows the depositional environment of the studied coal samples (Figure 9).

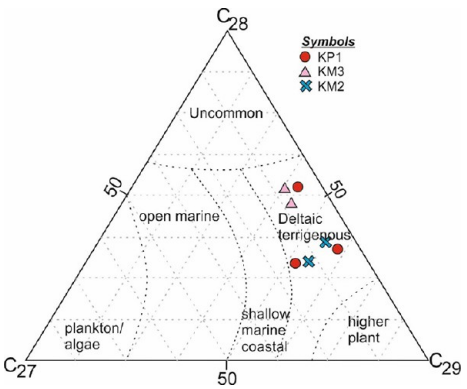

Figure 9. Ternary plot of steranes showing depositional facies. (adapted with permission from ref 89 . Copyright 2021 ACS.,[89,90])

DBT, a sulfur-containing compound, and its methyl homologues methyl dibenzothiophenes (MDBT) are shown in Figure 5d. DBTs present low values in coal extracts, indicating

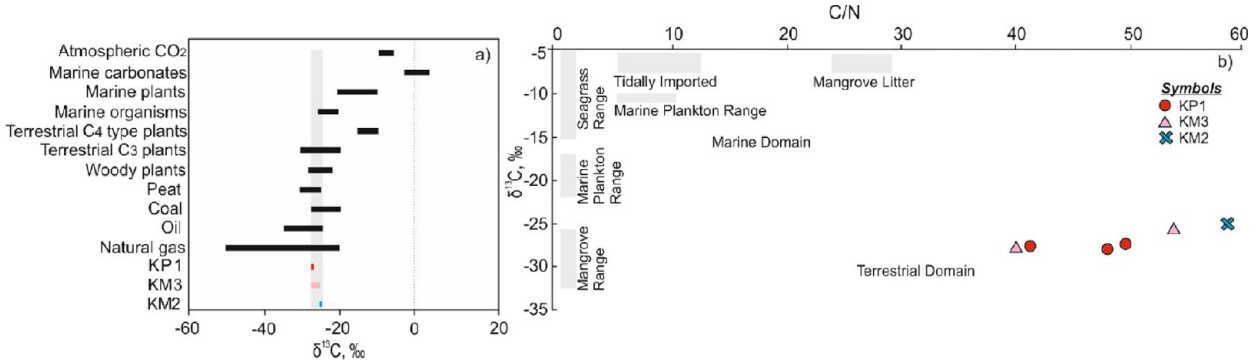

Figure 7. (a) $\delta^{13}C$ concentrations of some reference materials and (b) C/N ratio to $\delta^{13}C$ values for Soma-Manisa coal samples. (Adapted with permission from.[61] Copyright ACS 2023.,[60,61]).

https://doi.org/10.1021/acsomega.3c06635
ACS Omega 2023, 8, 47974−47990

dominant terrestrial facies.[91] The sulfur content of the analyzed samples varies and presents high values (Table 5). The low values of DBT values but variable sulfur contents in the coal samples suggest the variability in the Ph of the paleo-swamp.[92] In addition, low Gammacerane index, low C_{23} TT/(C_{23} TT + C_{30} H) ratio (between 0.02 and 016), absence of pregnane, and C_{29}/(C_{28} + C_{29}) MA steroid ratios greater than 0.5[20] suggest no marine influence. High TOC/S ratios also support the absence of a marine influence (Table 5). Therefore, the sulfur content and pyrite content are compatible, indicating the presence of inorganic sulfur (Figure 6).

Oils from marine environments have high DBT/P ratios, while oils from marine shale and most lacustrine rocks have low ratios.[93] The DBT/P ratios of the studied coal extracts (Table 4) are between 0.29 and 1.02. This indicates a strong input of terrestrial organic matter. The variable abundance of DBTs in all samples is indicative of possible suboxic and oxic conditions prevailing during deposition.

In Soma-Manisa field coal samples, huminite group macerals (KP1:29−68%, KM3:45−66%, KM2:59−78%), which are generally derived from woody tissues of roots, stems, and leaves,[35] are dominant whereas liptinite (KP1:1−6%, KM3:3−6%, KM2:3−10%) and inertinite (KP1:3−11%, KM3:5−17%, KM2:5−12%) group macerals are present at different rates in all seam samples (Figure 10). The presence of inertinites and liptinites in the studied coals indicates the presence of a paleo-swamp affected by water table fluctuations.[47]

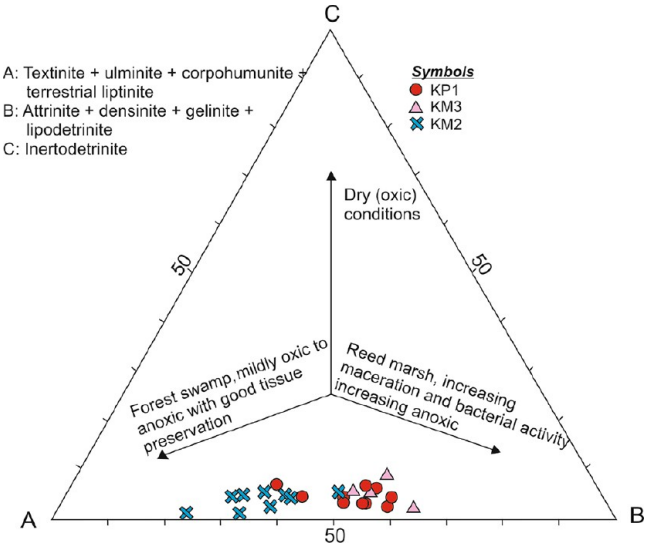

Figure 10. Ternary diagram showing peat-forming conditions and facies- maceral associations in the study area. (Adapted with permission from.[94] Copyright 2022 ACS.,[94,95]).

For coaly lithotypes, petrography-based VI, GWI, TPI, and GI facies indicators provide important information about the paleoenvironment in which the peat formed. In the studied coal samples, the KP1 and KM3 seams are characterized by VI values below 2, while the KM2 seam has VI values less than 5 (Table 6). This indicates that as the depth increases from the upper seam to the lower seam, the vegetative material changes and the dominant flora changes from herbaceous peat forming to woody plants. Low to medium GWI and VI values indicate that peat formed under mesotrophic and partially rheotrophic conditions.[46] High GWI and high TPI values are indicative of wet conditions, while low GWI and low TPI values are indicative of dry conditions of peat formation. Most of the analyzed samples have a high-value range between 0.5 and 5 for TPI and a medium−high-value range between 1 and 10 for GI, indicating that the coal samples were deposited in a wet condition of peat formation. The TPI-GI facies diagram shows that the analyzed coals in the TPI-GI facies diagram vary from the upper seam to the lower seam, from a limnic−limnotelmatic to a limnotelmatic−telmatic environment, and from an open swamp to a lacustrine−upper deltaic environment (Figure11a,b).

5.2. Thermal Maturity Assessment of Organic Matter.

The average random huminite reflectance (%Ro) values used as a parameter of degree of coalification ranged between 0.36 and 0.47% in the KP1 seam, between 0.44 and 0.47% in the KM3 seam, and between 0.45 and 0.49% in the KM2 seam, indicating sub-bituminous coal.[85] Tmax, PI data (Table 1), and %Ro values indicate that the coals in all three seams are immature in terms of thermal maturity and did not yet reach onset of oil expulsion (Figure 2).

The ratio of odd carbon number *n*-alkanes to even carbon number *n*-alkanes (OEP) can be used to determine thermal maturity.[20,39,40] In all three seams, high (>1) OEP data indicate the immature−early mature range.

Ts is lower than Tm in the KP1, KM3, and KM2 seams. While the Ts/(Ts+Tm) ratio increases with maturity,[45,98,99] the moretane/hopane ratio decreases with maturity (about 0.8 for immature source rock and <0.15 for mature source rock).[100−102] A high moretane/hopane ratio and a low Ts/(Ts+Tm) ratio characterize the immaturity of the studied coals. The 22S/(22S +22R) (C_{32}) homohopane ratio also increases with increasing maturity and reaches equilibrium in the range of 0.57−0.62.[100] The 22S/(22S+22R) (C_{32}) homohopane isomerization ratios of the examined samples are in the range 0.08−0.26, indicating the immature stage, which has not reached equilibrium. The $\beta\beta/(\beta\beta+\alpha\alpha)$ sterane ratio increases with maturation and reaches equilibrium in the range of 0.67−71.[74,87,103,104] The $\beta\beta/(\beta\beta+\alpha\alpha)$ sterane ratio was found to be low (<0.44) in the studied coals (Table 3).

The concentrations of aromatic compounds such as phenanthrenes, dibenzothiophenes, and their structural isomers are nowadays attracting more and more attention as maturity indicators of coals and shale source rocks.[105] The aromatic isomer ratios and indices used in this study are reported in Table 4. The methylphenanthrene index (MPI-1) is the most widely used molecular maturity parameter based on aromatic hydrocarbons and depends on the relative stability of isomers.[106] MPI-1 and MPI-1* ratios in the samples gave similar values (<1) indicating immaturity.[107] MA(I)/MA(I + II) and TA(I)/TA(I + II) steroid ratios increase from 0 to 100% with increasing maturity. MA(I)/MA(I + II) (between 0.02 and 0.09) and TA(I)/TA(I + II) (between 0.07 and 0.28) steroid maturity ratios of the studied coals were determined at very low levels, indicating the immature state of the coals (Table 4). The methyldibenzothiophene ratio (MDR), another maturity parameter calculated on the basis of methylbenzothiophene (MDBT) isomers, generally increases with increasing maturity.[108] In the studied samples, the MDR exhibited low values between 0.46 and 0.62 (Table 4), representing the immature phase.

6. CONCLUSIONS

Significant new results on hydrocarbon potentials, organic matter sources, and depositional environments of Miocene-aged coals from the Deniş (KP1 and KM3 seams) and Soma (KM2

https://doi.org/10.1021/acsomega.3c06635
ACS Omega 2023, 8, 47974−47990

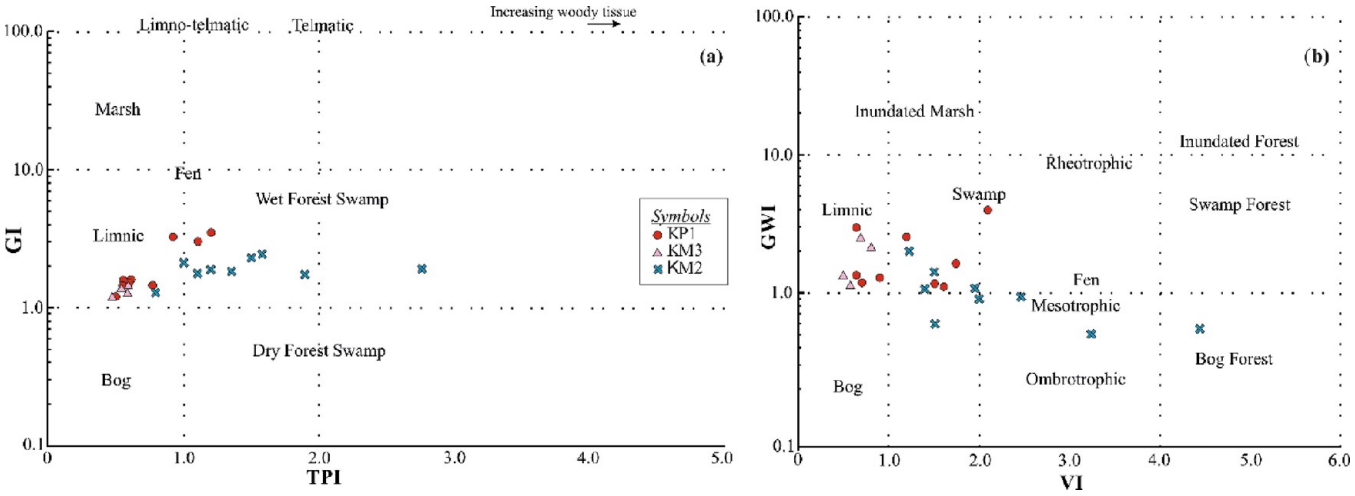

Figure 11. (a) GI vs TPI plot and (b) GWI vs VI plot of the Soma-Manisa coal samples. (adapted with permission from. ref 96. Copyright ACS 2021.,[47,96,97])

seam) Formations in the Soma-Manisa Basin are presented by using multiple analytical methods.

Rock-Eval pyrolysis results indicate that the studied coal samples are gas-prone and have not reached the maturity threshold for first gas generation and the onset of oil expulsion.

Huminite reflectance, Tmax, and saturated-aromatic biomarker indices indicate that the organic matter in KP1, KM3, and KM2 coals are thermally immature and suggest that Soma-Manisa coal has reached the sub-bituminous rank in the study area.

The *n*-alkane distributions and carbon isotopic data in the KP1-upper seam, KM3-middle seam, and KM2-lower seam coal samples indicate that terrestrial organic matter is dominant in the samples. According to TOC/N, Paq, and VI values, the dominant flora varies from the upper seam to the lower seam, indicating a change from emerged organic matter to submerged/floating organic matter abundance. According to Pwax, ACL values, it has been determined that from the upper seam to the lower seam, it has changed from moderately humid climatic conditions to humid and rainy climatic conditions. The low gammacerane index and relatively high Pr/Ph values of Soma-Manisa coals indicate that the low homohopane index developed in an oxic-suboxic depositional environment, in a terrestrial environment where there is no marine influence; TPI and GI values show that it varies from a limnotelmatic−limnotelmatic environment to a limnotelmatic−telmatic environment from the upper seam to the lower seam, from an open swamp to a lacustrine−upper deltaic environment. The variations in C_{29} and C_{28} sterane dominance and *n*-alkane distributions in the coal samples suggest that the depositional environments of the KM3 seam and the upper part of the KM2 seam occasionally changed to a lacustrine environment.

AUTHOR INFORMATION

Corresponding Author

Selin Karadirek − *Department of Geological Engineering, Akdeniz University, Antalya 07058, Turkey;* orcid.org/0000-0003-4829-600X; Email: selinhokerek@akdeniz.edu.tr

Complete contact information is available at: https://pubs.acs.org/10.1021/acsomega.3c06635

Notes

The author declares no competing financial interest.

ACKNOWLEDGMENTS

This study was financially supported by the Akdeniz University Research Unit (FBA-2019-4500). The author would like to thank General Directorate of Turkish Coal Enterprises for contributions of fieldwork and Prof. Dr. Orhan Ozcelik, Dr. Neslihan Unal Kartal for their valuable comments. The author would also like to thank to anonymous reviewers and the editor for their valuable comments.

REFERENCES

(1) *TKI Turkish Coal Enterprises Annual Report 2022*; Turkish Coal Enterprises: Ankara, Turkey Ankara, Turkey, 2023.

(2) MENR *Türkiye National Energy Plan*; Republic of Türkiye Ministry of Energy and Natural Resources: Ankara, Türkiye, 2022.

(3) Brinkmann, R.; Feist, R.; Marr, W. U.; Nickel, E.; Schlimm, W.; Walter, H. R. Geology of Soma Mountains (in Turkish). *Bull. Min. Res. Explor.* **1970**, *74*, 41−57.

(4) Nebert, K. Lignite-bearing Soma Neogene area, western Anatolia. *Bull. Miner. Res. Explor.* **1978**, *90*, 20−69.

(5) Cetin, A. *Soma dolaylarındaki linyitli Neojen sahalarının jeolojisi Ön Raporu (in Turkish; Neogene Geology of the Soma Lignite).*; 7047; M.T.A.: Ankara, Turkey, 1980.

(6) Gemici, Y.; Akyol, E.; Akgün, F.; Seçmen, O. Macro and micro fossil flora of Soma coal area. *Bull. Miner. Res. Explor.* **1991**, *112*, 161−178.

(7) Karayigit, A. I. Thermal effects of a basaltic intrusion on the soma lignite bed in west Turkey. *Energy Sources* **1998**, *20* (1), 55−66.

(8) Karayigit, A. I.; Gayer, R. A.; Querol, X.; Onacak, T. Contents of major and trace elements in feed coals from Turkish coal-fired power plants. *Int. J. Coal Geol.* **2000**, *44* (2), 169−184.

(9) Inci, U. Depositional evolution of Miocene coal successions in the Soma coalfield, western Turkey. *Int. J. Coal Geol.* **2002**, *51* (1), 1−29.

(10) Karayigit, A. I. In petrography and Facies Analysis of the Miocene Soma Coals, Manisa, Turkey, In *Proceedings of the 57th Meeting of the International Committee for Coal and Organic Petrology (ICCP)*; ICCP: Patras, Greece, Sept 21−27, 2005; Patras, Greece, 2005; p 12.

(11) Karayigit, A. I.; Bulut, Y.; Karayigit, G.; Querol, X.; Alastuey, A.; Vassilev, S.; Vassileva, C. Mass balance of major and trace elements in a coal-fired power plant. *Energy Sources Part A-Recovery Util. Environ. Eff.* **2006**, *28* (14), 1311−1320.

(12) Bulut, Y.; Karayigit, A. I. petrography of feed coals in the Soma power plant, Manisa, Turkey. *Energy Sources Part A-Recovery Util. Environ. Eff.* **2006**, *28* (16), 1447−1459.
(13) Tan, T.; Ertürk, I.; Pekmezci, F.; Altınay, A. *Manisa-Soma-Eynez İzmir-Kınık-Yaylaköy Sahası (in Turkish; Study Report of Manisa-Soma-Eynez, İzmir-Kınık-Yaylaköy Basins)*; TKI: Ankara, Turkey, 2010.
(14) Tercan, A. E.; Unver, B.; Hindistan, M. A.; Ertunc, G.; Atalay, F.; Unal, S.; Killioglu, Y. Seam modeling and resource estimation in the coalfields of western Anatolia. *Int. J. Coal Geol.* **2013**, *112*, 94−106.
(15) Hokerek, S.; Ozcelik, O. In *Organic facies characteristics of the Miocene Soma Formation (Lower Lignite Succession-KM2), Soma Coal Basin, western Turkey*, European Geosciences Union General Assembly 2015 - Division Energy, Resources and Environment, (EGU), Austria Center Vienna, Vienna, Australia, Apr 12−17; Elsevier Science Bv: Austria Center Vienna, Vienna, Australia, 2015; pp 27−32.
(16) Yasar, E. K. (Manisa-Türkiye) Kömürlerinin Organik Petrografik, Organik Jeokimyasal Özellikleri ve Gaz Depolama Kapasiteleri (in Turkish; Organic Petrographic, Organic Geochemical Characteristics of Soma (Manisa-Turkey) Coals and Their Gas Store Capacity); MSc. Thesis, Istanbul University: Istanbul, Turkey, 2011.
(17) Karadirek, S.; Ozcelik, O. Organic Geochemical Characteristics and Depositional Environment of the Soma-Eynez (Manisa) Coals, Western Anatolia, Turkey. *Energy Fuels* **2019**, *33* (2), 677−690.
(18) Oskay, R. G.; Bechtel, A.; Karayiğit, A. İ. Mineralogy, petrography and organic geochemistry of Miocene coal seams in the Kinik coalfield (Soma Basin-Western Turkey): Insights into depositional environment and palaeovegetation. *Int. J. Coal Geology* **2019**, *210*, 103205.
(19) Bechtel, A.; Sachsenhofer, R. F.; Markic, M.; Gratzer, R.; Lucke, A.; Puttmann, W. Paleoenvironmental implications from biomarker and stable isotope investigations on the Pliocene Velenje lignite seam (Slovenia). *Org. Geochem.* **2003**, *34* (9), 1277−1298.
(20) Peters, K. E.; Walters, C. C.; Moldowan, J. M. *The Biomarker Guide. II. Biomarkers and Isotopes in Petroleum Systems and Earth History*; 2nd ed.; Cambridge University Press 2005; p 475−1155.
(21) Mathews, R. P.; Chetia, R.; Agrawal, S.; Singh, B. D.; Singh, P. K.; Singh, V. P.; Singh, A. Early Palaeogene Climate Variability Based on n-alkane and Stable Carbon Isotopic Composition Evidenced from the Barsingsar Lignite-bearing Sequence of Rajasthan. *J. Geol. Soc. India* **2020**, *95* (3), 255−262.
(22) Chetia, R.; Mathews, R. P.; Singh, P. K.; Sharma, A. Conifer-mixed tropical rainforest in the Indian Paleogene: New evidences from terpenoid signatures. *Paleogeogr. Paleoclimatol. Paleoecol.* **2022**, *596*, No. 110980, DOI: 10.1016/j.palaeo.2022.110980.
(23) Ojha, S.; Singh, P. K. Petrogenesis and Evolution of Tharad Coals of Cambay Basin, Gujarat (Western India): An Insight. *J. Geol. Soc. India* **2023**, *99* (5), 675−687.
(24) Hossain, H. M. Z.; Sampei, Y.; Hossain, Q. H.; Yamanaka, T.; Roser, B. P.; Sultan-Ul-Islam, M. Origin of organic matter and hydrocarbon potential of Permian Gondwana coaly shales intercalated in coals/sands of the Barapukuria basin. *Int. J. Coal Geol.* **2019**, *212*, 103201.
(25) He, D.; Huang, H.; Arismendi, G. G. n-Alkane distribution in ombrotrophic peatlands from the northeastern Alberta, Canada, and its paleoclimatic implications. *Palaeogeogr. Palaeoclimatol. Palaeoecol.* **2019**, *528*, 247−257.
(26) Li, L.; Jin, J. H.; Quan, C.; Oskolski, A. A. First record of Podocarpoid fossil wood in South China. *Sci. Rep* **2016**, *6*, 32294 DOI: 10.1038/srep32294.
(27) Zhang, Y. D.; Su, Y. L.; Liu, Z. W.; Yu, J. L.; Jin, M. Lipid biomarker evidence for determining the origin and distribution of organic matter in surface sediments of Lake Taihu. *Eastern China. Ecol. Indic.* **2017**, *77*, 397−408.
(28) Hos-Cebi, F. Organic geochemical characteristics and paleoclimate conditions of the Miocene coals at the Can-Durali (Canakkale). *J. Afr. Earth Sci.* **2017**, *129*, 117−135.
(29) İncı, U. Lignite and carbonate deposition in Middle Lignite succession of the Soma Formation, Soma coalfield, western Turkey. *Int. J. Coal Geol.* **1998**, *37* (3−4), 287.
(30) Karayigit, A. I.; Whateley, M. K. G. Properties of a lacustrine subbituminous (k1) seam, with special reference to the contact metamorphism. *Soma-Turkey. Int. J. Coal Geol.* **1997**, *34* (1−2), 131−155.
(31) Nebert, K. *Geology of the lignite-bearing Basin (Soma-Manisa) located in the South of Bakircay*; Rap., no. 3019; M.T.A.: Ankara, Turkey, 1959.
(32) Espitalie, J.; Deroo, G.; Marquis, F. Rock-Eval pyrolysis and its applications. *Rev. Inst. Fr. Pet.* **1985**, *40* (5), 563−579.
(33) Peters, K. E. Guidelines for evaluating petroleum source rock using programmed pyrolysis. *AAPG Bull.* **1986**, *70* (3), 318−329.
(34) Lafargue, E.; Marquis, F.; Pillot, D. Rock-Eval 6 applications in hydrocarbon exploration, production, and soil contamination studies. *Rev. Inst. Fr. Pet.* **1998**, *53* (4), 421−437.
(35) Sykorova, I.; Pickel, W.; Christanis, K.; Wolf, M.; Taylor, G. H.; Flores, D. Classification of huminite - ICCP system 1994. *Int. J. Coal Geol.* **2005**, *62* (1−2), 85−106.
(36) Taylor, G. H.; Teichmüller, M.; Davis, A.; Diessel, C. F. K.; Littke, R.; Robert, P. *Organic Petrology*; Gebrüder Borntraeger: Berlin, 1998; p 704.
(37) Wu, P.; Dujie, H.; Cao, L.; Zheng, R.; Wei, X.; Ma, X.; Zhao, Z.; Chen, J. paleoenvironment and Organic Characterization of the Lower Cretaceous Lacustrine Source Rocks in the Erlian Basin: The Influence of Hydrothermal and Volcanic Activity on the Source Rock Quality. *ACS Omega* **2023**, *8* (2), 1885−1911.
(38) Sykes, R.; Snowdon, L. R. Guidelines for assessing the petroleum potential of coaly source rocks using Rock-Eval pyrolysis. *Org. Geochem.* **2002**, *33* (12), 1441−1455.
(39) Bray, E. E.; Evans, E. D. Distribution of n-paraffins as a clue to recognition of source beds. *Geochim. Cosmochim. Acta* **1961**, *22* (1), 2−15.
(40) Scalan, R. S.; Smith, J. E. An improved measure of odd-even predominance in normal alkanes of sediment extracts and petroleum. *Geochim. Cosmochim. Acta* **1970**, *34* (5), 611.
(41) Zheng, Y. H.; Zhou, W. J.; Meyers, P. A.; Xie, S. C. Lipid biomarkers in the Zoige-Hongyuan peat deposit: Indicators of Holocene climate changes in West China. *Org. Geochem.* **2007**, *38* (11), 1927−1940.
(42) Bourbonniere, R. A.; Meyers, P. A. Sedimentary geolipid records of historical changes in the watersheds and productivities of Lakes Ontario and Erie. *Limnol. Oceanogr.* **1996**, *41* (2), 352−359.
(43) Ficken, K. J.; Li, B.; Swain, D. L.; Eglinton, G. An n-alkane proxy for the sedimentary input of submerged/floating freshwater aquatic macrophytes. *Org. Geochem.* **2000**, *31* (7−8), 745−749.
(44) Zhou, W. J.; Xie, S. C.; Meyers, P. A.; Zheng, Y. H. Reconstruction of late glacial and Holocene climate evolution in southern China from geolipids and pollen in the Dingnan peat sequence. *Org. Geochem.* **2005**, *36* (9), 1272−1284.
(45) Moldowan, J. M.; Sundararaman, P.; Schoell, M. Sensitivity of biomarker properties to depositional environment and or source input in the lower Toarcian of Southwest Germany. *Org. Geochem.* **1986**, *10* (4−6), 915−926.
(46) Calder, J. H.; Gibling, M. R.; Mukhopadhyay, P. K. Peat Formation in a Westphalian-B Piedmont Setting, Cumberland Basin, Nova-Scotia - Implications For The Maceral-Based Interpretation of Rheotrophic and Raised Paleomires. *Bull. Soc. Geol. Fr.* **1991**, *162* (2), 283−298.
(47) Diessel, C. F. K. *Coal-bearing Depositional Systems*; Springer-Verlag: Berlin- Heidelberg, 1992; p 721.
(48) Kalkreuth, W.; Kotis, T.; Papanicolaou, C.; Kokkinakis, P. The geology and coal petrology of a Miocene lignite profile at Meliadi mine, Katerini. *Greece. Int. J. Coal Geol.* **1991**, *17* (1), 51−67.
(49) Peters, K. E.; Cassa, M. R., Applied Source-Rock Geochemistry. In *The Petroleum System. From Source to Trap*; American Association of Petroleum Geologists: Tulsa, 1994; pp 93−12.
(50) Singh, V. P.; Singh, B. D.; Mathews, R. P.; Singh, A.; Mendhe, V. A.; Singh, P. K.; Mishra, S.; Dutta, S.; Shivanna, M.; Singh, M. P. Investigation on the lignite deposits of Surkha mine (Saurashtra Basin,

https://doi.org/10.1021/acsomega.3c06635
ACS Omega 2023, 8, 47974−47990

Gujarat), western India: Their depositional history and hydrocarbon generation potential. *Int. J. Coal Geol.* **2017**, *183*, 78−99.
(51) Singh, P. K.; Singh, V. K.; Rajak, P. K.; Mathur, N. A study on assessment of hydrocarbon potential of the lignite deposits of Saurashtra basin, Gujarat (Western India). *Int. J. Coal Sci. Technol.* **2017**, *4* (4), 310−321.
(52) Singh, P. K.; Singh, V. K.; Rajak, P. K.; Singh, M. P.; Naik, A. S.; Raju, S. V.; Mohanty, D. Eocene lignites from Cambay basin, Western India: An excellent source of hydrocarbon. *Geosci. Front.* **2016**, *7* (5), 811−819.
(53) Meyers, P. A. Preservation of elemental and isotopic source identification of sedimentary organic-matter. *Chem. Geol.* **1994**, *114* (3−4), 289−302.
(54) Lamb, A. L.; Wilson, G. P.; Leng, M. J. A review of coastal palaeoclimate and relative sea-level reconstructions using delta C-13 and C/N ratios in organic material. *Earth-Sci. Rev.* **2006**, *75* (1−4), 29−57.
(55) Inoue, T.; Suzuki, N.; Hasegawa, H.; Saito, H. Differential transportation and deposition of terrestrial biomarkers in middle Eocene fluvial to estuarine environments, Hokkaido. *Japan. Int. J. Coal Geol.* **2012**, *96*−*97*, 39−48.
(56) Sofer, Z. Stable carbon isotope compositions of crude oils - application to source depositional-environments and petroleum alteration. *AAPG Bull.* **1984**, *68* (1), 31−49.
(57) Collister, J. W.; Wavrek, D. A. delta C-13 compositions of saturate and aromatic fractions of lacustrine oils and bitumens: Evidence for water column stratification. *Org. Geochem.* **1996**, *24* (8−9), 913−920.
(58) Koralay, D. B. Deposition characteristics of pliocene coals in the denizli region (SW Turkey) via organic petrography, geochemistry, and stable isotope composition. *J. Nat. Gas Sci. Eng.* **2020**, *84*, No. 103619.
(59) Singh, P. K.; Singh, M. P.; Prachiti, P. K.; Kalpana, M. S.; Manikyamba, C.; Lakshminarayana, G.; Singh, A. K.; Naik, A. S. Petrographic characteristics and carbon isotopic composition of Permian coal: Implications on depositional environment of Sattupalli coalfield, Godavari Valley. *India. Int. J. Coal Geol.* **2012**, *90*, 34−42.
(60) Florentine, C., Stable Isotope Analysis of Sedimentary Organic Matter From Bioluminescent Bays in Vieques, Puerto Rico, Suggest a Link Between Mangrove Decay and Bioluminescence. In *20th Annual Keck Symposium*; College of Wooster: Wooster, OH, 2007.
(61) Yu, T.; Wu, Z.; Guo, R.; Zhang, G.; Zhang, Y.; Shang, F.; Chen, L. Hydrocarbon Generation from Low-Mature Saline Lacustrine Sediments Studied Using Machine Learning and Chemometric Methods: The Succession of the Sikeshu Sag, Junggar Basin. *NW China. ACS Omega* **2023**, *8* (11), 10314−10334.
(62) Sun, Y. Z.; Qin, S. J.; Zhao, C. L.; Li, Y. H.; Yu, H. C.; Zhang, Y. Organic geochemistry of semianthracite from the Gequan Mine, Xingtai Coalfield. *China. Int. J. Coal Geol.* **2013**, *116*, 281−292.
(63) Hanson, A. D.; Zhang, S. C.; Moldowan, J. M.; Liang, D. G.; Zhang, B. M. Molecular organic geochemistry of the Tarim basin, northwest China. *AAPG Bull.* **2000**, *84* (8), 1109−1128.
(64) Han, J.; McCarthy, E. D.; Hoeven, W. V.; Calvin, M.; Bradley, W. H. Organic geochemical studies, II. A preliminary report on the distribution of aliphatic hydrocarbons in algae, in bacteria, and in a recent lake sediments. *Proc. Natl. Acad. Sci. U.S.A.* **1968**, *59*, 29−33.
(65) Tuo, J. C.; Ma, W. Y.; Zhang, M. F.; Wang, X. B. Organic geochemistry of the Dongsheng sedimentary uranium ore deposits. *China. Appl. Geochem.* **2007**, *22* (9), 1949−1969.
(66) Cranwell, P. A.; Eglinton, G.; Robinson, N. Lipids of aquatic organisms as potential contributors to lacustrine sediments. *Org. Geochem.* **1987**, *11* (6), 513−527.
(67) Corrigan, D.; Kloos, C.; O'Connor, C. S.; Timoney, R. F. Alkanes From 4 Species of Sphagnum-Moss. *Phytochemistry* **1973**, *12* (1), 213−214.
(68) Aichner, B.; Herzschuh, U.; Wilkes, H. Influence of aquatic macrophytes on the stable carbon isotopic signatures of sedimentary organic matter in lakes on the Tibetan Plateau. *Org. Geochem.* **2010**, *41* (7), 706−718.
(69) Bingham, E. M.; McClymont, E. L.; Valiranta, M.; Mauquoy, D.; Roberts, Z.; Chambers, F. M.; Pancost, R. D.; Evershed, R. P. Conservative composition of n-alkane biomarkers in Sphagnum species: implications for palaeoclimate reconstruction in ombrotrophic peat bogs. *Org. Geochem.* **2010**, *41* (2), 214−220.
(70) Bush, R. T.; McInerney, F. A. Leaf wax n-alkane distributions in and across modern plants: Implications for paleoecology and chemotaxonomy. *Geochim. Cosmochim. Acta* **2013**, *117*, 161−179.
(71) Bechtel, A.; Oberauer, K.; Kostic, A.; Gratzer, R.; Milisavljevic, V.; Aleksic, N.; Stojanovic, K.; Gross, D.; Sachsenhofer, R. F. Depositional environment and hydrocarbon source potential of the Lower Miocene oil shale deposit in the Aleksinac Basin (Serbia). *Org. Geochem.* **2018**, *115*, 93−112.
(72) Eglinton, G.; Hamilton, R. J. Leaf Epicuticular Waxes. *Science* **1967**, *156* (3780), 1322−1335.
(73) Liu, W. G.; Yang, H.; Wang, H. Y.; An, Z. S.; Wang, Z.; Leng, Q. Carbon isotope composition of long chain leaf wax n-alkanes in lake sediments: A dual indicator of paleoenvironment in the Qinghai-Tibet Plateau. *Org. Geochem.* **2015**, *83*−*84*, 190−201.
(74) Peters, K. E.; Moldowan, J. M. *The biomarker guide. Interpreting molecular fossils in petroleum and ancient sediments*; Prentice-Hall: NJ, 1993; p 363.
(75) Simoneit, B. R. T.; Cardoso, J. N.; Robinson, N. An assessment of terrestrial higher molecular-weight lipid compounds in aerosol particulate matter over the south-atlantic from about 30-degrees-s-70-degrees-s. *Chemosphere* **1991**, *23* (4), 447−465.
(76) Cranwell, P. A. Chain-length distribution of n-alkanes from lake sediments in relation to post-glacial environmental change. *Freshwater Biology* **1973**, *3*, 259−265.
(77) Zhou, J. B.; Zhuang, X. G.; Alastuey, A.; Querol, X.; Li, J. H. Geochemistry and mineralogy of coal in the recently explored Zhundong large coal field in the Junggar basin, Xinjiang province. *China. Int. J. Coal Geol.* **2010**, *82* (1−2), 51−67.
(78) Didyk, B. M.; Simoneit, B. R. T.; Brassell, S. C.; Eglinton, G. Organic geochemical indicators of paleo-environmental conditions of sedimentation. *Nature* **1978**, *272* (5650), 216−222.
(79) Powell, T. G.; McKirdy, D. M. Relationship between ratio of pristane to phytane, crude-oil composition and geological environment in Australia. *Nature-Physical Science* **1973**, *243* (124), 37−39.
(80) Volkman, J. K.; Maxwell, J. R., Acyclic isoprenoids as biological markers. In *Biological Markers in the Sedimentary Record Johns*; R. B., Ed. Elsevier: Amsterdam, 1986; pp 1−42.
(81) Kara-Gulbay, R. Organic geochemical and petrographical characteristics of coal bearing Oligo-Miocene sequence in the Oltu-Narman Basin (Erzurum). *NE Turkey. Int. J. Coal Geol.* **2015**, *149*, 93−107.
(82) Yalcın Erik, N. paleoenvironment characteristics and hydrocarbon potential of the Lower Miocene bituminous shales in Sivas Basin (Central Anatolia, Turkey). *Arab. J. Geosci.* **2016**, *9* (1), 15.
(83) Kara-Gulbay, R.; Korkmaz, S.; Yaylalı-Abanuz, G.; Erdogan, M. Organic Gechemistry and Depositional Environment of the Oltu Gemstone (Coal) in the Erzurum Area, NE Anatolia. *Turkey. Energy Fuels* **2018**, *32* (2), 1451−1463.
(84) Hunt, J. M. *Petroleum geochemistry and geology*; W.H. Freeman and Company: New York, 1996.
(85) Tissot, B.; Welte, D. H. *Petroleum formation and occurence*; Springer-Verlag: Berlin, 1984; p 699.
(86) Bocker, J.; Littke, R.; Hartkopf-Froder, C.; Jasper, K.; Schwarzbauer, J. Organic geochemistry of Duckmantian (Pennsylvanian) coals from the Ruhr Basin, western Germany. *Int. J. Coal Geol.* **2013**, *107*, 112−126.
(87) Waples, D.; Machihara, T. *Biomarkers for Geologists: A Practical Guide to the Application of Steranes and Triterpanes in Petroleum Exploration*; American Association of Petroleum Geologists: Tulsa, 1991; p 91.
(88) Hegazi, A. H.; El-Gayar, M. S. Geochemical characterization of a biodegraded crude oil, Assran field, Central Gulf of Suez. *J. Pet. Geol.* **2009**, *32* (4), 343−355.

https://doi.org/10.1021/acsomega.3c06635
ACS Omega 2023, 8, 47974−47990

(89) Guo, W.; Chen, G.; Li, Y.; Li, Y.; Zhang, Y.; Zhou, J.; Han, W.; Xu, X.; Ma, Y.; Dang, H. Factors Controlling the Lower Radioactivity and Its Relation with Higher Organic Matter Content for Middle Jurassic Oil Shale in Yuqia Depression, Northern Qaidam Basin, China: Evidence from Organic and Inorganic Geochemistry. *ACS Omega* **2021**, *6* (11), 7360−7373.
(90) Huang, W. Y.; Meinschein, W. G. Sterols as Ecological Indicators. *Geochim. Cosmochim. Acta* **1979**, *43* (5), 739−745.
(91) Radke, M.; Welte, D. H.; Willsch, H. Distribution of alkylated aromatic-hydrocarbons and dibenzothiophenes in rocks of the Upper Rhine graben. *Chem. Geol.* **1991**, *93* (3−4), 325−341.
(92) Markic, M.; Sachsenhofer, R. F. Petrographic composition and depositional environments of the Pliocene Velenje lignite seam (Slovenia). *Int. J. Coal Geol.* **1997**, *33* (3), 229−254.
(93) Petersen, H. I.; Nytoft, H. P.; Ratanasthien, B.; Foopatthanakamol, A. Oils from Cenozoic rift-basins in central and northern Thailand: Source and thermal maturity. *J. Pet. Geol.* **2007**, *30* (1), 59−77.
(94) Das, P. R.; Mendhe, V. A.; Kamble, A. D.; Sharma, P.; Shukla, P.; Varma, A. K. Petrographic and Geochemical Controls on Methane Genesis, Pore Fractal Attributes, and Sorption of Lower Gondwana Coal of Jharia Basin. *India. ACS Omega* **2022**, *7* (1), 299−324.
(95) Mukhopadhyay, P. K., petrography of selected Wilcox and Jockson Group lignites fromTertiary of Texas. In *Geology of Gulf Coast Lignites*; Finkelman, R. B.; Casagrade, D. J., Eds. Annu. Meet. Geological Society ofAmerica, Coal Geology Division, Field Trip, 1986; pp 126−145.
(96) Lu, Q.; Qin, S.; Xu, F.; Chang, X.; Wang, W. Maceral and Organic Geochemical Characteristics of the Late Permian Coals from Yueliangtian Mine, Guizhou. *Southwestern China. ACS Omega* **2021**, *6* (4), 3149−3163.
(97) Kalaitzidis, S.; Bouzinos, A.; Papazisimou, S.; Christanis, K. A short-term establishment of forest fen habitat during Pliocene lignite formation in the Ptolemais Basin, NW Macedonia. *Int. J. Coal Geol.* **2004**, *57* (3−4), 243−263.
(98) Seifert, W. K.; Michael Moldowan, J. Applications of steranes, Terpanes and mono-aromatics to maturation, migration and source of crude oils. *Geochim. Cosmochim. Acta* **1978**, *42* (1), 77−95.
(99) Aquino Neto, F. R.; Trendel, J. M.; Restle, A.; Connan, J.; Albrecht, P. A., Occurrence and formation of tricyclic and tetracyclic Terpanes in sediments and petroleums. In *Advances in Organic Geochemistry Bjory*; M., Ed. John Wiley & Sons:: New York, 1983; pp 659−676.
(100) Seifert, W. K.; Moldowan, J. M. The effect of thermal stress on source-rock quality as measured by hopane stereochemistry. *Phys. Chem. Earth* **1980**, *12*, 229−237.
(101) Cornford, C.; Morrow, J. A.; Turrington, A.; Miles, J. A.; Brooks, J., Some Geological Controls on Oil Composition in the U.K. North Sea. In *Petroleum Geochemistry and Exploration of Europe*, Brooks, J., Ed. Blackwell Scientific Publications:: Oxford London Edinburgh Boston Melbourne, 1983; pp 175−194.
(102) Kvenvolden, K. A.; Simoneit, B. R. Hydrothermally derived petroleum - Examples from Guaymas Basin, Gulf of California, and Escanaba Trough, Northeast Pacific-Ocean. *AAPG Bul.* **1990**, *74* (3), 223−237.
(103) Seifert, W. K.; Moldowan, J. M., Use of biological markers in petroleum exploration. In *Methods in Geochemistry and Geophysics*, Johns, R. B., Ed. Elsevier: Amsterdam, 1986; pp 261−290.
(104) Marzi, R.; Rullkotter, J., Qualitative and quantitative evolution and kinetics of biological marker transformations: laboratory experiments and application to the Michigan Basin. In *Biological Markers in Sediments and Petroleum*; Moldowan, J. M.; Albrecht, P.; Philp, R. P., Eds. Prentice-Hall: Englewood Cliffs, NJ, 1992; pp 18−41.
(105) Ogala, J. E.; Akaegbobi, M. I. Using aromatic biological markers as a tool for assessing thermal maturity of source rocks in the Campano-Maastrichtian Mamu Formation, southeastern Nigeria. *Earth Sci. Res. J.* **2014**, *18* (1), 51−62.
(106) Radke, M.; Welte, D., The methylphenanthrene index (MPI): a maturity para-meter based on aromatic hydrocarbons. In *Adv. Org. Geochem.*; Bjorey, M., Ed. J. Wiley & Sons: Chichester, 1983; pp 504−512.
(107) Radke, M.; Horsefield, B.; Littke, R.; Rullkötter, J., Maturation and petroleum generation. In *Migration of hydrocarbons in sedimentary basins*; Dohgez, B., Ed. Academic Press: London, 1997; pp 649−665.
(108) Radke, M.; Welte, D. H.; Willsch, H. Maturity parameters based on aromatic-hydrocarbons - influence of the organic-matter type. *Org. Geochem.* **1986**, *10* (1−3), 51−63.

https://doi.org/10.1021/acsomega.3c06635
ACS Omega 2023, 8, 47974−47990